DR. JOSE C. SÁNCHEZ GARRIDO (Orcid ID : 0000-0003-1524-7391)

Article type : Original Article

Dynamics of anchovy and sardine populations in the Canary Current off NW Africa: responses to environmental and climate forcing in a climate-to-fish ecosystem model

José C. Sánchez-Garrido[1], Jerome Fiechter[2], Kenneth A. Rose[3], Francisco E. Werner[4], Enrique N. Curchitser[5]

[1]*Physical Oceanography Group, Department of Applied Physic II, University of Málaga, Campus de Teatinos s/n, 29071, Málaga, Spain*

[2] *Institute of Marine Sciences, University of California, Santa Cruz, CA 95064, USA*

[3] *University of Maryland Center for Environmental Science, Horn Point Laboratory, PO Box 775, Cambridge, MD 21613, USA*

[4] *NOAA Fisheries, 1315 East-West Highway, Silver Spring, MD 20910, USA*

[5]*Department of Environmental Sciences, Rutgers University, 14 College Farm Road, New Brunswick, NJ 08901, USA*

Keywords: Canary Current; anchovy; sardine; population dynamics; biophysical modeling; IBM; NAO; AMO; upwelling; wind.

Corresponding author: José C. Sánchez-Garrido (jcsanchez@ctima.uma.es)

Abstract

A 50-year-long (1958–2008) historical simulation of a climate-to-fish ecosystem model for anchovy (*Eugralis encrasicolus*) and sardine (*Sardina pilchardus*) populations in the upwelling ecosystem off NW Africa is revisited and analyzed. Anchovy and sardine annual adult abundances were correlated at interannual and decadal time scales in the historical run.

A three-step analysis method applied unraveled the environmental and life stage-specific drivers underlying the bottom-up mechanisms responsible for the simulated variability in anchovy and sardine populations. Changes in anchovy adult abundance were primarily controlled by larval survival, prey availability, and local upwelling strength, whereas sardine adult abundance was controlled by age-1 growth affecting age-2 fecundity and egg production via prey availability. Despite different diet preferences, the common sensitivity of anchovy and sardine to prey availability had a synchronizing effect on the two populations, with both anchovy and sardine doing better during years of higher plankton biomass and colder ocean temperatures. Analysis of potential links with modes of climate variability showed that anchovy dynamics were more tightly connected to the AMO while sardine dynamics were correlated to the NAO. This difference stemmed from the vulnerability of the anchovy population to enhanced coastal upwelling causing increased larval drift mortality. Finally, based on an earlier, similar modeling study for the Californian anchovy and Pacific sardine, we argue that the relatively warmer habitat off NW Africa compared to the coastal region off central California, is a key feature explaining synchronous populations in the Canary Current versus out-of-phase anchovy and sardine cycles in the California Current.

1. Introduction

Forage fishes (e.g., anchovy, sardine, and herring) represent up to 20% of the world fisheries catch (FAO, 2019). This group of fishes, often dominated by anchovy and sardine species, are most abundant in coastal upwelling regions where they represent a major connection between plankton and multiple upper trophic level organisms, including a variety of larger fish, seabird, and marine mammal species. Large interannual fluctuations of anchovy and

sardine landings, and other small pelagic species, reflect a strong sensitivity of these fishes to changes in their habitats (Schwartzlose et al., 1999). It is generally assumed that variability in anchovy and sardine populations results mainly from bottom-up effects (e.g., climate-driven forcing), with top-down effects (i.e., fishing and predation) playing a secondary role (Checkley et al., 2017). Due to the commercial and ecological importance of these species, elucidating the possible responses of anchovy and sardine dynamics to climate variation is of primary scientific interest (Chavez et al., 2003, Lindegren et al., 2013).

A question that has attracted much attention in the small pelagic fishery literature is the origin of alternating cycles between anchovy and sardine in eastern boundary upwelling systems (EBUS), suggested in landing records of the 20th century (Lluch-Cota et al., 2013, Alheit & Ñiquen 2004). One of such systems is the California Current System (CCS), in which ups and downs of anchovy and sardine have been traditionally associated with warm and cold phases of the eastern Pacific (Chavez et al., 2003, Zwolinski & Demer 2012). Recently, McClatchie el al. (2017) has shown from 500-year paleorecord that alternation of anchovy and sardine off Southern California is not longstanding and that abundances of anchovy and sardine appear positively correlated over long time scales (centuries). An EBUS in which no clear alternation cycles between anchovy and sardine have been detected is the Canary Current System off NW Africa (CanCS; Alheit et al., 2009; also see Braham & Corten 2015, Thiaw et al., 2017, and Brochier et al., 2018). Here, sardine (*Sardina pilchardus*) is permanently dominant over anchovy (*Eugralis encrasicolus*) and the catches of the two species appear positively correlated (Sánchez-Garrido et al., 2019).

Understanding the drivers and underlying mechanisms for anchovy and sardine cycles (whether alternating or synchronous) is difficult because of the inherent limitations of long-term physical, biochemical, and ecological times series observations. Anchovy and sardine, and fish populations in general, are influenced by multiple factors that vary on a range of temporal and spatial scales, making it difficult to definitively partition trends and variation to specific drivers and processes (Rose 2000). Such limitations are partially alleviated with complex end-to-end ecosystem models that, by combining circulation, lower-, and upper-trophic submodels into a single model, provide a numerical tool for identifying and quantifying the causes of underlying dynamics of fish populations (Fulton et al., 2010, Rose et al., 2010).

Rose et al. (2015) described the fundamental processes included in a fully-coupled end-to-end ecosystem model for anchovy and sardine in the California Current system (CCS). In a companion paper, Fiechter et al. (2015a) showed how results of a multidecadal (1964–2008) simulation of the CCS can be analyzed to reveal environmental and climate drivers for alternating cycles between the Northern anchovy and Pacific sardine. The model was subsequently used to simulate prey effects on salmon growth (Fiechter et al., 2015b) and sea lion bioenergetics (Fiechter et al., 2016). Further work with the model in the CCS analyzed the connections between climate variability and sardine recruitment (Politikos et al., 2017) and the response of the sardine and anchovy system to a pronounced climate perturbation such as the North Pacific 1976-1977 regime shift (Nishikawa et al., 2019). Recently, Sánchez-Garrido et al. (2019) demonstrated the flexibility of the formulation used by Rose et al. (2015) by adapting the CCS end-to-end model to the CanCS. Modification of key parameters capturing distinctive traits and behavior of the European sardine and anchovy (reproductive phenology, optimum temperatures, and allometric coefficients) resulted in synchronous variability of these two species. Moreover, fish biomasses were found to vary at interannual and decadal temporal scales similar to historical landing records, suggesting a mechanistic response of anchovy and sardine to the regional climate variability represented in the circulation and lower trophic submodels. A first analysis of the simulation focused on years of high and low recruitment and revealed a particular sensitivity of the anchovy and sardine to the survival of feeding early life stage individuals (larvae and juveniles) and, in addition, to egg production for sardine. The co-variability of sardine and anchovy was then explained by the common dependence of early life stage survival and egg production on the overall prey availability generated by the lower trophic submodel.

While Sánchez-Garrido et al. (2019) offered insights into the synchronous dynamics of anchovy and sardine in the CanCS, they did not fully analyze the results of their simulation for cause-and-effect understanding of how climate forcing influenced the population responses of anchovy and sardine. Namely, they did not show how multi-year fluctuations of the ocean circulation and physics propagate through the food web, from lower-trophic levels to fish early life stages, and ultimately to the adult populations. This paper addresses this gap by revisiting the simulation of Sánchez-Garrido et al. (2019) following the approach used in Fiechter et al. (2015a) for the CCS. The objective of this paper is twofold. First, we use the modeling results to provide a comprehensive view of the mechanistic response of anchovy and sardine to climate variability in the CanCS. We pay particular attention to the biological

impact of the North Atlantic Oscillation (NAO) and the Atlantic Multidecadal Oscillation (AMO) that have been previously related to the variability of clupeid populations in the Northeast Atlantic (Arístegui et al., 2006, Alheit et al., 2014). The second objective is to compare analogous simulations of the CanCS and the CCS, highlighting the distinctive features of the two systems that ultimately lead to in- and out-of-phase low-frequency cycles of sardine and anchovy populations. Such a comparison is possible because very similarly structured end-to-end ecosystem models and analysis methods of the results were used in both locations.

2. End-to-end ecosystem model

The end-to-end (here climate-to-fish) model combines a regional circulation submodel, a lower trophic nutrient-phytoplankton-zooplankton (NPZ) submodel, and a multispecies individual-based submodel for the fish species. All these components are coupled and run over the same computational grid. For a comprehensive description of the model, the reader is referred to Rose et al. (2015); here we summarize the main model features and the set up for the present application to the CanCS. Further details of the model configuration, calibration strategy, and skill assessments of the specific simulation for the CanCS analyzed here can be found in Sánchez-Garrido et al. (2019).

2.1 Circulation submodel

The circulation submodel is based on the Regional Ocean Modeling System (ROMS; Shchepetkin & McWilliams, 2005). A ROMS application covering the upwelling regions off NW Africa and the Iberian Peninsula was implemented (7.5ºN-50ºN, 38ºW-1ºW; Figure 1). The horizontal grid resolution was set to a constant value of 12 km, which was computationally affordable and allowed for the generation of some eddy variability in the model — the internal Rossby radius is of the order of 30–40 km across the CanCS domain —. In the vertical dimension, the domain was discretized with 38 vertical terrain-following levels with increasing resolution towards the free surface. The model bathymetry was derived from the ETOPO-1 database (Amante and Eakins 2009). The NPZ and fish submodels were run within the same 3-D computational grid as the circulation submodel.

Horizontal eddy diffusivity and viscosity coefficients were both set to 5 m^2s^{-1}, while vertical turbulent mixing and dissipation were calculated following the nonlocal K-profile parameterization of Large et al. (1994). Initial and lateral boundary values for sea water

temperature, salinity, velocity, and sea surface height, updated monthly, were derived from the Simple Ocean Data Assimilation reanalysis data set (SODA 2.0.2; Carton & Giese, 2008). Atmospheric forcing fields were obtained from the Common Ocean-Ice Reference Experiment database (CORE-2; Large & Yeager, 2008), which is based on the NCEP/NCAR reanalysis (Kalnay et al., 1996) and included 6-hourly wind velocity, air temperature, sea level pressure, specific humidity, daily shortwave and downward longwave radiation, and monthly precipitation. Surface wind stress, upward longwave radiation, sensible and latent heat fluxes were calculated from the bulk formulae described in Large & Yeager (2008).

2.2 Lower trophic NPZ submodel

The NEMURO NPZ model (Kishi et al., 2007, 2011; Werner et al., 2007) was used for the lower trophic levels. In its simplest version, the one employed here, NEMURO incorporates 11 state variables: nitrate, ammonium, and silicic acid as possible limiting nutrients, two phytoplankton functional groups (nanoplankton and a diatom-like larger organism), and three zooplankton groups (micro-, meso-, and a larger predatory zooplankton); the remaining state variables are particulate organic nitrogen, dissolved organic nitrogen, and particulate silica detritus pools.

Initial and boundary values for nutrients (nitrate and silicic acid) were obtained from monthly climatological values of the World Ocean Atlas 2001 (Conkright & Boyer, 2002). Initial and boundary conditions for ammonium, phytoplankton, zooplankton, and detritus were constant at 0.1 mmol Nm^{-3}. Based on the similarity between the CanCS and the CCS, both being EBUS, and the similarity of the scales of the numerical models implemented, we adopted the same NEMURO configuration as in Fiechter et al. (2015a) and then introduced modifications to capture distinctive characteristics of the CanCS NPZ food web. Because large phytoplankton cells do not appear clearly dominated by diatom species in the CanCS, with the exception of very coastal habitats (Arístegui et al., 2009), no limitation of silicic acid was imposed for the otherwise diatom-like large phytoplankton species of the model. As part of the calibration, the two phytoplankton groups were also given the same photoinhibition coefficients to better match the spatial patterns in surface chlorophyll (Sánchez-Garrido et al., 2019).

2.3 Fish IBM

The IBM incorporates a coastal anchovy-like species, a more oceanic sardine-like species, and a generic predatory fish species. For a detailed description of the IBM, specific parameter values for anchovy and sardine, and model skill assessment based on landings (FAO, 2001; FAO, 2012) and acoustic surveys observations in the CanCS (Arístegui et al., 2009), the reader is referred to Sánchez-Garrido et al. (2019); here we summarize the main features of the model.

The IBM follows the super-individual approach of Scheffer et al. (1995) in which a fixed number of individuals, referred to as super-individuals, represent a variable amount of identical fish individuals (super-individual's worth). Changes in population abundance are accounted for by variations of super-individual's worth so that the fish population can be represented with reduced computer memory. The sole purpose for the predatory fish was to exert density-dependent mortality on anchovy and sardine, so only its movement and consumption were simulated, and its abundance (i.e., its total worth) was held constant.

The IBM simulates the full life cycle of anchovy and sardine: individuals are tracked through the life stages of egg, yolk-sac larva (hereinafter ysac), feeding larva, juvenile, and adult. Development from egg-to-ysac and from ysac-to-feeding larva was dependent on the sea water temperature, while metamorphosis (feeding larva-to-juvenile) occurred based on an individual's length. Juveniles automatically became immature adults (recruited) on their first birthday, which occurred on January 1 for all individuals. Maturation was generally attained during the incoming year based on fish length. Growth in weight depended on consumption, respiration, and reproduction, and was calculated hourly based on fish bioenergetics and a functional response relationship using local sea water temperature and zooplankton concentrations from the NEMURO submodel. Consumption was calculated as

$$C = C_m W P, \quad (1)$$

where W is fish weight, $C_m = a_c W^{b_c} F(T)$ is the maximum consumption rate incorporating allometric (a_c and b_c constants) and a temperature effect $F(T)$, and P (also called P-value in bioenergetics literature) is a non-dimensional measure of food availability. P is interpreted as the fraction of maximum consumption due to food limitation, and varies among individuals and each hour due to local zooplankton concentrations, species- and life stage-specific feeding efficiencies and vulnerability parameters for each zooplankton type (e.g., larvae cannot eat predatory zooplankton; anchovy adults prefer larger prey than sardine). P was

computed as a type II functional response using the concentrations of the three zooplankton groups from the NEMURO submodel for which the individual fish had assigned vulnerabilities greater than zero (Rose et al., 1999). Fish length was updated hourly from fish weight and it was not allowed to decrease, enabling poor body conditions for the individuals (i.e., skinny fish).

Anchovy and sardine in the model incurred natural, starvation, and predation mortality. Natural mortality rates were fixed and life-stage dependent, and together with predation, resulted in a decrease of super-individuals' worth. Starvation mortality occurred when individuals' weight dropped below a certain fraction of the expected weight for their length (from weight–length relationships; 50% for larvae and 40% for juveniles and adults) and led to the removal of the super-individual from the simulation. The fishing fleet submodel (i.e., harvest) developed by Rose et al. (2015) and used in Fiechter et al. (2015a) was not incorporated because our focus here was exclusively on bottom-up controls of the fish populations.

Adult individuals spawned in batches over defined spawning periods: anchovy from April 10th to August 15th and sardine from November 1st to April 10th. A spawner initiated a batch spawning event if it experienced appropriate sea water temperature (within the range 16ºC–21.5ºC for anchovy and 16.5ºC–20.5ºC for sardine; from SST observations at spawning sites), if it had sufficient resting time since the last batch was released, and if it had sufficient energy available from recent consumption of prey. Eggs, ysacs, and larvae were advected by ocean currents and were assumed to remain in the top layer (i.e., sea surface). Juvenile and adult individuals moved following a kinesis approach (Humston et al., 2004; Watkins & Rose 2013) using temperature and food availability (indexed by *P*) as cues. Optimum temperatures for kinesis corresponded to average spawning temperatures (18.75ºC anchovy; 18.50ºC sardine). Kinesis was first applied in the horizontal direction and then in the vertical. The position of every individual was updated hourly and their maximum allowed swimming speed was three body lengths per second. Movement of anchovy individuals entering deep waters (> 2000 m depth) was biased towards the coast to account for its coastal preference compared to sardine. The predatory fish moved according to a restricted-area search approach (Watkins & Rose, 2013) designed for predator individuals to effectively target adults and juveniles of sardine and anchovy.

Anchovy and sardine individuals were further classified into age classes. Early life stages (egg-to-juvenile) were labeled as age-0 and adults were age-1 class or older. On January 1 each year, young-of-the-year juveniles automatically became both (immature) adults and age-1 individuals. Super-individuals having effectively zero worth, due to starvation or having reached the maximum permitted age of 9 years, were removed from the simulation. The removal for low worth and starvation was evaluated daily. The removal for old age was done once per year on January 1 and the freed up super-individuals were then used to keep track of the next year's young. This enabled a constant number of super-individuals to be in the simulation at all times, with their summed worths showing population-level fluctuations in abundance.

All model outputs were necessarily adjusted for the worths of all super-individuals. For example, population abundance of adults was the sum of the worths of adult super-individuals, and mean length was a weighted average of the lengths of super-individuals with worths as the weighting factors. Survival fraction for a particular life stage each year was calculated as the summed worth of individuals whenever they exited the life stage divided by the summed worth of individuals whenever they entered it.

3. Historical simulation

The end-to-end model simulated the period 1958–2008 (Sánchez-Garrido et al., 2019). The first 6 years of the simulation, covering the lifespan of the first generation of fish, were discarded from the analysis to minimize effects of initial conditions.

Spatial distributions of anchovy and sardine averaged over the simulation reflected their biological traits and phenology and were similar across life stages for each species but differed between anchovy and sardine (Figure 2). All life stages of anchovies concentrated in coastal regions off northern Morocco, namely north of Cape Ghir (Figure 1), and in the Gulf of Cádiz (36ºN-37ºN). Sardine were distributed over a broader area than anchovy and extended farther offshore into the basin. In general, sardine were located at lower latitudes than anchovy, becoming most abundant in the vicinity of Cape Blanc and Cape Juby. These spatial distributions partially result from the spawning seasonality of the two species. During the summer (anchovy spawning season), anchovy locate in feeding grounds in the northern part of the CanCS as trade winds shift to the north (Sánchez-Garrido et al., 2019). Hence, early life stages of anchovy (top row of Figure 2) are also commonly found around this

region. The same reasoning can be applied to sardine (autumn-to-winter spawner) with the trade winds moving southward towards the end of the year to explain their tendency to be found in the central and southern parts of the CanCS. For both anchovy and sardine, adult abundances were more highly concentrated inshore along the coast than other life stages, and the effects of advection by the prevailing southward upwelling current is seen with the more dispersed and southward locations of anchovy eggs and larvae relative to juveniles and adults (see also Brochier et al., 2011).

Anchovy and sardine exhibited noticeable interannual and longer-scale variability in their adult population abundances (Figure 3). The two populations were positively correlated (r=0.41), with both reaching maximums in abundance by the late 1970s and the mid-1990s and minimums in the early 1970s and late 1980s.

4. Analysis of historical simulation

4.1. Analysis procedure

To explore the linkages between climate, environmental (i.e., physics and prey availability), and biological (i.e., growth, survival and reproduction of anchovy and sardine) variability in the simulation (Figure 3), we conducted a three-step analysis of the model results. Our strategy was similar to that used by Fiechter et al. (2015a) for their analysis of a historical simulation of anchovy and sardine in the CCS.

The first step identifies the primary biological drivers influencing the interannual variability of sardine and anchovy adult populations. Because predation mortality was small compared to natural mortality and did not play a major role in controlling adult abundance (Sánchez-Garrido et al., 2019), we focused exclusively on the dynamics of early life stages as drivers of adult abundances. Specifically, we analyzed the effects of age-0 survival and annual egg production on adult abundances. Age-0 survival fraction was calculated as the number of juveniles becoming sub-adults each January 1 (i.e., recruits) divided by the annual egg production.

Because egg production is potentially two-way related to adult abundance (i.e., more adults typically lead to more eggs and more eggs lead to more adults), cause-effect relationships were determined according to a lead-lag correlation analysis. For example, a maximum correlation over all lags obtained for the number of adults in a given year and the number of

eggs spawned the year prior indicates dependence of adult abundance upon egg production, rather than the opposite. On the other hand, because adult abundance can only be influenced by age-0 survival but not in the other direction (i.e., adults do not feed on age-0 individuals and age-0 mortality is density-independent), age-0 survival was only considered as a potential biological driver if it was positively correlated with adult abundance at negative lags (e.g., if the number of adults was correlated with age-0 survival the year prior).

As part of the Step 1 analysis, the specific life stages and age classes playing the greatest role in the adult population dynamics were also identified. Importance of stages and age classes for sardine and anchovy was based on early life stage (egg/ysac, larval, juvenile, and age-0) survival and, additionally for sardine, influence of age-1 weight and growth and age-2 growth on age-2 fecundity (eggs/ind). We used age-2 fecundity rather than age-2 egg production to remove the effects of abundance and to isolate whether body weight and growth of sardine were affecting egg production.

The second step of the analysis investigates the environmental conditions (food, ocean temperature) responsible for the key biological processes identified as important to determining adult abundances in Step 1. For example, we identified larval stage survival as important determinant of age-0 survival, which in turn, affected adult abundance of anchovy. We therefore examined food and temperature conditions experienced by anchovy larvae and compared the environmental conditions among years of anomalously high and low larval stage survival. These conditions were then connected to the spatial patterns of environmental variability generated by ROMS and NEMURO.

The third and final step relates simulated sardine and anchovy cycles to known regional modes of climate variability in the North Atlantic. Our interpretation of the role of climate variability is based on the correlations between the environmental patterns associated with variations of anchovy and sardine (from the second step) and reported indices for the climate modes. We summarized environmental conditions generated by ROMS and NEMURO submodels with an Empirical Orthogonal Function (EOF) decomposition, and related the three EOFs (SST, total phytoplankton, total zooplankton) to anchovy and sardine survival and growth, and also related the EOFs to multiple climate indices. This enabled us to try to relate simulated important anchovy and sardine processes with indices from outside the model that reflected general environmental conditions.

The analyses used the historical simulation results on the hourly dynamics of super-individuals to generate a suite of output variables, which were then used in Steps 1-3. The response and explanatory variables for the analyses of model output for Steps 1-3 are summarized in the online supporting information of this paper. All variables from the model simulation were computed using adjustments for the different worths of super-individuals, and variables were averaged to obtain single values for each year.

4.2. Step 1: Biological control on adult populations

4.2.1 Age-0 survival versus egg production

For anchovy, age-0 survival played a role in determining the abundance of the population (Step 1a) because adult abundance correlated the highest (r=0.43) with age-0 survival the year prior (i.e., at lag -1 year; Figure 4, top-left panel, and Table 1). The correlation was also positive at -2 year lag (r=0.36), whereas it was negligible at 0 and +1 year lag (), which was expected because adults do not influence age-0 survival in the model. Conversely, adult abundance was highly correlated with egg production at all lags (Figure 4, bottom-left panel, and Table 1), as expected from the direct relationship between number of adults and the population's reproductive output. Causality was elucidated from the fact that adult abundance (i) correlated the highest with egg production one year later (r=0.90; +1 year lag), and (ii) correlated more closely with the egg production the same year (r=0.86; 0 year lag) than the year before (r=0.75; -1 year lag). These lagged relations indicate that variation in adult anchovy abundance determined future egg production more than egg production strongly determined future adult abundance.

For sardine, adult abundance was uncorrelated with age-0 survival (Step 1a) the preceding years (r=-0.07 and 0.01 at lags -2 and -1 year), implying absence, or at most, a weak cause-effect relationship (Table 2 and Figure 4, right panels). Regarding egg production, the correlation between adult sardine abundance and egg production was the highest at -1 year lag (r=0.75; with egg production one year prior), and progressively decreased for 0 to +1 year lags (r=0.64 to r=0.54), indicating that egg production was a driver of changes in sardine adult abundance.

Altogether, the correlation analysis revealed different biological drivers for anchovy and sardine adult population abundances. While adult anchovy abundance variability was primarily controlled by age-0 survival, egg production emerged as the main process affecting

adult abundance of sardine. Anchovy and sardine adult abundances were also affected by other processes, but to a lesser extent. For example, the fact that age-0 survival did not correlate with adult sardine abundance in subsequent years does not exclude the possibility for recruitment to be associated with age-0 survival in specific years. This was indeed the case during 2000-2007 when age-0 survival of sardine (at -1 year lag) was more closely correlated with adult sardine abundance than with egg production (Figure 4); while the opposite (age-0 survival unimportant) was true for anchovy during 1964-1972.

4.2.2 Key life stages and age classes

Stage-specific survival fractions were compared with age-0 survival (Figure 5) to identify key early life stages (Step 1b). For anchovy, age-0 and larval stage survivals were highly correlated (r=0.90), whereas the correlations for sardine between age-0 survival and early life stage survivals (Figure 5) were weak (maximum of r=0.26) and even negative (juveniles: r=-0.66). Therefore, the variability of age-0 survival (and that of the anchovy adult population but not sardines) was largely determined by survival during the larval stage.

For sardine, age-0 survival variability (Step 1b) was mainly associated with juvenile and larval stage survivals (r=0.8 and r=0.39, respectively) although, as Figure 4 and Section 4.2 showed, age-0 survival was not the primary driver for changes in adult abundance. Rather, adult sardine abundance responded to egg production (Step 1a), which was highly correlated with adult abundance at -1year lag (r=0.75; Table 2). The highest correlation between age-specific egg production and adult abundance (Step 1c, Figure 6) corresponded to the age-2 class (r=0.62, Table 2). The reproductive output of the age-2 class was also the largest among all age classes with a yearly production of eggs (27% of the total annual production).

To remove the effect of adult abundance on age-2 egg production (Step 1d), we focused on fecundity (eggs/ind) of age-2 adults (Figure 7) rather than on the total reproductive output of this age class. Fecundity of age-2 explains part of the age-2 annual egg production (r=0.45; Table 3) and was strongly related to age-1 growth (r=0.79) lagged -1 year (Figure 7 and Table 3). Whereas larval survival affected age-0 survival that determined adult abundance for anchovy, age-1 growth was most tightly connected to age-2 fecundity that determined egg production and adult abundances for sardine.

4.3. Step 2: Environmental control on biological processes

Based on the results from Step 1, good or bad years for anchovy and sardine were defined (Step 2a) as years for which anchovy age-0 survival or sardine age-1 growth were above or below one standard deviation their respective long-term means (Figure 8). All remaining years for anchovy (not good or bad) were considered normal years for anchovy and all remaining years not good or bad for sardine were considered normal for sardine. Anchovy had 7 bad and 8 good years (29 normal years), while sardine had 6 bad and 6 good years (32 normal years). Consistent with the synchronous variability of anchovy and sardine in the CanCS (Figure 3), there were some years that were good or bad for both species (good: 1974, 1999, 2007; bad: 1969, 1995, 1997).

The Lagrangian approach of the IBM allowed tracking of ocean temperatures and feeding conditions (P) experienced every hour by each individual fish in space and time. We exploited this feature to examine conditions experienced by all age-0 anchovy each year during normal and anomalous years (Step 2b, Figure 9). Anchovy larvae, whose survival primarily explained the annual variability of age-0 survival, generally experienced colder than normal-year averaged temperature during good years and warmer than normal-year temperatures during bad years (bottom rows in Figure 9); and the same was true for eggs with ysac (top row in Figure 9). Because egg and ysac development rates increase with temperature and so also its survival fraction, the fact that seawater was colder (warmer) than normal during good (bad) years confirms the secondary role of egg and ysac survival on anchovy dynamics. On the other hand, anchovy larvae, which experienced colder temperatures in good years and warmer temperatures in bad years, also encountered higher than normal-year food in good years and lower than normal-year food in bad years (bottom row of Figure 9).

The relative role of temperature and food on anchovy larval survival was further evaluated (Step 2d) using the consumption formulation from the model bioenergetics. Because larval survival is mediated by an individuals' growth rate (i.e., how quickly an individual can grow out of the high mortality larval stage), we evaluated the changes in temperature and prey availability in bad and good years on larval consumption rate (Table 4). The mean temperature anomaly experienced by anchovy larvae during good and bad years was -0.13ºC and 0.22ºC, respectively, which based on eq. (1) implied a deviation of consumption of 0.02% with respect to its average value in normal years (ΔC_T in Table 4). For food effects, P anomalies (0.02-0.03) led to changes in consumption rate two orders of magnitude greater

than due to temperature (ΔC_P=3.5% during good years and ΔC_P=-2.3% during bad years; Table 4), revealing a stronger dependence of anchovy larval survival on differences in zooplankton between good and bad years compared to temperature.

Similar to anchovy larvae, sardine age-1 individuals experienced (Step 2c) waters colder than normal and with better feeding conditions during good years, and the opposite during bad years (Figure 10). Temperature anomalies (Step 2d) were somewhat greater than for age-1 sardine than for anchovy larvae (0.3-0.4ºC; Table 5) that led to larger deviations of age-1 consumption with respect to normal years: ΔC_T =0.5% (good years) and ΔC_T =-1.1% (bad years). However, like anchovy larvae, the effects of temperature on consumption for age-1 sardines were still smaller than the effects of food anomalies, ΔC_P=2.4% (good years) and ΔC_P=-2.0% (bad years). This suggests that sardine age-1 growth (and therefore age-2 fecundity) between good and bad years was, like anchovy larvae, regulated primarily by food abundance with a small but consistent effect of temperature.

4.4 Step 3: Connection with climate variability

4.4.1 Eulerian environmental patterns

Direct analysis of ROMS and NEMURO outputs (Step 3a) provide a broad picture of the prevailing environmental conditions during good and bad years for age-0 anchovy survival and age-1 growth of sardines. For anchovy, years of high age-0 survival (good years) displayed generally cold SSTs and increased prey availability when viewed basin-wide (Figure 11). The greatest SST and plankton concentration anomalies occurred in the region between Cape Juby and Cape Blanc, and were more moderate, or even locally of opposite sign, further north near Cape Ghir (preferred anchovy habitat). These patterns are consistent with opposite anomalies of the prevailing upwelling-favorable winds in the northern and southern parts of the system (upper-right panel of Figure 11): in the context of widespread cold and productive waters, weakening of coastal upwelling around Cape Ghir tends to lessen local SST and plankton anomalies, which, in contrast, are amplified to the south as a result of intensified upwelling.

Anchovy age-0 survival, controlled by larval survival, is hence maximized under locally weakened upwelling. This finding supports the results of Sánchez-Garrido et al. (2019) who showed that upwelling in northern Morocco was weaker than normal during years of high anchovy recruitment, and that upwelling conditions can be related to the vulnerability of

anchovy larvae to drift mortality (mortality resulting from transport of larvae away from the spawning region and into less productive waters where they cannot sustain growth). Anchovy larvae in the model simulation found good feeding conditions north of Cape Ghir as the trade winds shift north during the summer (the spawning season for anchovy), whereas to the south (downstream) food is only abundant within a narrow coastal strip running up to Cape Blanc (central lower panel of Figure 9). Off Cape Blanc and farther south food becomes abundant again, but the warmer waters (SST>24ºC) of this region constrain larval survival (Sánchez-Garrido et al., 2019). According to this hypothesis, anchovy larvae benefit from reduced local wind and upwelling by those conditions favoring retention on the shelf, as well as from a general increase of plankton abundance that improve survival chances of drifting individuals. Pronounced weakening of the upwelling-favorable winds, however, causes high mortality to anchovy larvae because the associated drop of primary productivity and food supply offsets the positive effect of larval retention. Indeed, years of low age-0 anchovy survival (bad years) show a marked and generalized decline of upwelling-favorable winds, warm SSTs, and decrease of plankton in the CanCS.

For sardine (Step 3b), environmental patterns during anomalous years (high and low age-1 growth) were generally similar to those for anchovies but with enhanced temperature and food anomalies, particularly nearshore (Figure 12). Because age-1 individuals are not subject to drift mortality (i.e., they can swim toward preferred locations), there is no evidence in the simulation of local upwelling relaxation (i.e., weaker winds) affecting sardine habitat during good years, as opposed to good years for anchovy. Instead, age-1 growth of sardine depended fundamentally on overall prey availability, which is related more readily with wind and upwelling (stronger is always better).

4.4.2 EOF patterns and climate indices

The patterns associated with anchovy age-0 survival and sardine age-1 growth (Figs. 11 and 12) resemble leading patterns of physical and biochemical variability identified from an Empirical Orthogonal Function (EOF) decomposition of the ROMS and NEMURO outputs (Step 3c, Figure 13). EOFs were estimated separately for SST, total phytoplankton (nano- plus microplankton groups), and total zooplankton (sum of micro-, meso-, and a predatory groups) using time series of annual average values at each horizontal cell. Domain-wide changes of zooplankton abundance with enhanced nearshore concentrations are captured by the first EOF mode, and similar large-scale (but more spatially uniform) variation of SST and

phytoplankton are accounted for by their respective first and third EOF modes. Since these environmental patterns occur during anomalous years identified for anchovy and sardine, the corresponding EOF temporal amplitudes (Figure 13; right panels) can be used as proxies for the status of each species' adult populations (Step 3d). Indeed, anchovy and sardine abundance generally co-vary with the EOF temporal amplitudes, increasing or decreasing as the EOF amplitudes change sign (Figure 14).

The above EOF patterns (Step 3e) are further related to modes of regional and basin-scale climate variability (Figure 15 and Table 6): the NAO (Hurrell, 1995) and AMO (e.g., Trenberth & Shea, 2006). A positive NAO index indicates stronger than normal westerlies at mid-latitudes and strengthening of the Azores high. Colder-than-normal winter SST and upwelling-favorable wind stress off NW Africa have been also associated with a positive NAO phase (Marshall et al., 2001, Arístegui et al., 2006).

Examining our model results (Step 3e, Table 6), the NAO index correlates negatively with the first EOF mode for SST (r=-0.41) and the third EOF mode for phytoplankton (r=-0.42), indicating generally cold seawater and increased phytoplankton biomass north of Cape Blanc during positive NAO phases. The NAO index also correlates negatively with the leading mode for zooplankton (i.e., above-normal zooplankton biomass for positive NAO) but weakly (r=-0.27). The AMO index is SST-based and its pattern during positive (negative) phases displays anomalously warm (cold) SST over most of the North Atlantic (Alexander et al., 2014). Expectedly, the AMO index correlates positively with the first EOF mode for SST (r=0.59). In our model simulation, positive AMO phases are also associated with reduced phytoplankton biomass across the CanCS (r=0.52 for the third EOF mode for phytoplankton). In addition to the NAO and AMO, we also explored the Bakun Upwelling index at 30ºN (UI30N; in the middle of the domain), which correlates most highly with the leading zooplankton mode (r=-0.54), and the El Niño Southern Oscillation NIÑO 3.4 index, which generally exhibits weaker correlations with all EOF temporal amplitudes (r<0.38).

A direct comparison (Step 3f) between the above indices and the driving biological processes for anchovy (age-0 survival) and sardine (age-1 growth) during anomalous years (Figure 16) supports the correlations established using EOF modes, but also suggests a closer linkage between anchovy and the AMO (r=-0.65) and between sardine and the NAO (r=0.77). Such comparison also highlights the stronger dependence of sardine on upwelling-favorable winds than anchovy.

5. Differences with respect to the CCS populations

Our analyses identified different environmental and biological drivers for anchovy and sardine abundance variability than those identified for the CCS populations in Fiechter et al. (2015a), and offer an explanation for the observed sardine and anchovy synchronicity in the CanCS versus the asynchronicity in the CCS. Essentially, the out-of-phase variability of the CCS populations results from the different sensitivities of anchovy and sardine to food availability and to ocean temperatures (Fiechter et al., 2015a), combined with the fact that these two variables tend to be negatively correlated in upwelling systems. While anchovy strongly responded to local feeding conditions in the southern CCS (primary adult habitat) via age-1 growth and age-2 fecundity, sardine was most sensitive to domain-wide temperature variation controlling the survival of early life stages (and ultimately age-0 survival) (Figure 17). In the CanCS simulation, the co-variability of anchovy and sardine was driven primarily by their common sensitivity to the overall food supply, even if the underlying mechanisms were different for the two species.

The lack of importance of egg and yolk-sac survival (i.e., temperature dependence) on either anchovy or sardine dynamics is one of the main features distinguishing the CanCS simulation from the CCS simulation. This feature helps explain the qualitatively different coherence of the anchovy and sardine populations (i.e., in- and out-of-phase) and can be explained by the relatively warmer surface waters of the CanCS compared to the CCS. This temperature difference is partially attributed to the closer proximity of the CanCS to the tropics (30ºN versus 36ºN) and, with respect to fish, it appears to be further strengthened by the reproductive phenology of Northern anchovy and Pacific sardine in the CCS where both species spawn during the coldest months of the year (winter-to-spring). In our CanCS simulation, eggs and yolk-sac larvae experienced ocean temperatures about 4.5ºC warmer than in those reported in Fiechter et al. (2015a)'s CCS simulation (19.5ºC versus 14ºC), which results in faster egg/ysac development (40 h versus 80 h stage durations) and greater survival fractions (Figure 18). Consequently, eggs and yolk-sac larvae in the CCS simulation were more sensitive to changes in seawater temperature. Even though similar ranges of interannual temperature were experienced by eggs and ysac in the two systems (see box plots in Figure 18), the cooler conditions in the CCS result in greater variability of development time in the CCS due to the nonlinear dependence of development rate on temperature. Longer and greater variation in development times translates into more variation in egg and

ysac survival in the CCS. Thus, in relation to the mean, egg and yolk-sac larval survival exhibit higher interannual variation in the CCS compared to the CanCS simulation, potentially becoming more important in controlling population dynamics. In fact, among all the species, the greatest coefficient of variation (*CV*) for egg and yolk-sac larva survival corresponds to Pacific sardine (12.2% and 13.75%, respectively), which showed the strongest response to temperature. The same coefficients are roughly half for Northern anchovy (3.9% and 6.4%) and European sardine (5.6% and 5.2%), and even smaller for European anchovy (1.6% and 5.0%); all populations controlled more directly by biological processes associated with food availability (Figure 17).

6. Summary and Discussion

Combining physical, lower-trophic, and upper-trophic level submodels, end-to-end ecosystem models allow for the investigation of links between climate, environmental, and biological variability. The comprehensive approach of end-to-end models and their relatively high level of complexity and realism comes at the cost of having to deal with large amounts of information needed for inputs and extensive outputs. Our approach with the same model applied to two locations was to use a common framework and approach for analyzing the simulation outputs. This included repeating some of the details of the analysis to maintain consistency, such as the lagged correlation analysis and defining "good" and "bad" years. In this spirit, our paper reanalyzed the results of Sánchez-Garrido et al., (2019) in the CanCS based on the earlier work by Fiechter et al. (2015a) in the CCS. By doing so, we gained deeper insights into the population dynamics of anchovy and sardine within and across systems.

The analyses here support the conclusions of Sánchez-Garrido et al. (2019) regarding the common sensitivity of anchovy and sardine to food availability as the primary cause for their synchronous variability in the CanCS. We further elucidated that larval survival for anchovy and age-1 growth for sardine are the two main biological processes explaining this common sensitivity to food supply. The conclusion that good (bad) years for the two species coincide with years colder (warmer) than normal should therefore not be interpreted as a direct effect of temperature on fish, but rather as a consequence of the typical negative correlation existing between SST and plankton biomass in the CanCS (r=-0.66 for spatial averaged values). This finding applies to both species, and especially to anchovy; both species were much less sensitive to temperature fluctuations than food variation in the simulation (Tables 4 and 5).

Patterns of environmental conditions during anomalous years (good and bad) for sardine and anchovy corresponded roughly to leading EOF modes of variability summarized from the outputs of the ROMS and NEMURO submodels. Perfect agreement between EOF modes and anchovy and sardine patterns could not be established and differences among many of the anchovy and sardine results were too subtle to be unambiguously associated with distinct modes (unlike in the CCS study of Fiechter et al., 2015a). However, the EOF analysis reported here confirmed that variation of anchovy and sardine abundances were at least partly associated with basin-wide variability of plankton biomass and SST (Figure 14). In the CanCS system, as in the CCS simulation, model results enabled clear connections between broad-scale climate indices and biological variability of anchovy and sardine.

Our results concur with observational evidence provided in Alheit et al. (2014), who suggested that there was a close relation between the AMO and interannual variation in clupeids abundance in the Northeastern Atlantic (Figure 16). Alheit et al. (2014) assumed a negligible role of temperature as an environmental driver and proposed fluctuations of the subpolar gyre, echoed by the AMO index, as a candidate physical forcing of the fish population dynamics. Contractions of the subpolar gyre (and the concomitant expansions of the subtropical gyre) would lead to the intrusion of warm, low-nutrient and plankton-poor subtropical waters to the northeast. In contrast, expansions of the gyre would lead to conditions of cold, high-nutrient and plankton-rich subpolar waters. Noticeably, our results support the notion that the AMO's effect on anchovy and sardine would indeed not be mediated by temperature but rather by plankton. However, our results do not shed light on the specific large-scale changes of the North Atlantic circulation involved. Such changes are not obviously captured by our regional model, although their effects would be partially accounted for through the boundary conditions.

The NAO impact on anchovy and sardine is explained from the associated wind pattern in the Northeast Atlantic (Marshall et al., 2001; Visbeck 1998). Positive NAO phases are related to stronger coastal upwelling and enhanced food supply off NW Africa for both anchovy and sardine. Sardine benefited the most from enhanced upwelling in the simulation because age-1 growth is not strongly affected by offshore Ekman transport. In contrast, anchovy rely primarily on larval dispersal and survival, and did not always do well with intensified upwelling currents (and greater NAO values) (Figure 11 and 16). Overall, variation in annual sardine and anchovy populations were most tightly connected to the NAO and AMO,

respectively (Figure 11). ENSO, which has also been related to variability of clupeids off NW Africa (e.g., migration patterns of *Sardinella aurita*; López-Parages et al., 2020), seems to play a secondary role in the dynamics of anchovy and sardine in our model. The identified anchovy sensitivity to larval drift mortality also suggests that anchovy can be particularly vulnerable to future climate scenarios that project enhanced alongshore winds in EBUS (Bakun et al., 1990).

The relatively warmer temperatures experienced by anchovy and sardine in the CanCS simulation compared to the CCS simulation was a key feature leading to in-phase, instead of out-of-phase, variability in anchovy and sardine abundances. Of course, this result only applies to the CanCS and does not exclude the possibility for anchovy and sardine stocks exploiting similar temperature habitats to display out-of-phase abundance cycles. For example, reported spawning temperatures off Peru for anchovy are 16-18ºC and for sardine 19-22ºC (Schwartzlose et al., 1999, Sera & Tsukayama 1988), which are close to sea surface temperatures off NW Africa (Figure 18). Optimal spawning temperatures for Japanese anchovy and sardine, which also show alternating dominance cycles based on landings (Oozeki et al., 2019, Lluch-Cota et al., 2013), also range between 16-22ºC (Takasuka et al., 2008). Future modeling could focus on these ecosystems to identify other potential mechanisms for out-of-phase biological variability.

Our model of the CanCS is similar to the one implemented for CCS (Fiechter et al., 2015a), with only a few adjustments of parameter values to represent distinctive traits of the European sardine and anchovy populations off NW Africa. These adjustments mostly focused on reproductive phenology, optimum temperatures, and length-weight relationships (Sánchez-Garrido et al., 2019). These basic modifications capturing the essential characteristics of anchovy-like and sardine-like species in the CanCS, along with the environmental variability generated by ROMS and NEMURO in the Canary basin, were sufficient to lead to different population dynamics compared to their analogue species in the CCS. This minimum-change approach was adopted for two reasons. First, we maintained the basic model structure that would facilitate intersystem comparisons; and second, while many other changes could have been made, we only changed aspects for which we had high confidence or we thought important to capture the new species and system. For example, other potential processes affecting fish dynamics in the CanCS, such as cannibalism, intraguild predation, and migratory behavior, were neglected, and top-down effects were

simply represented with a single generic predatory species and without harvest. All these processes could help explain discrepancies between predicted and observed anchovy and sardine dynamics (Sánchez-Garrido et al., 2019). Abrupt dynamical shifts as the one recently observed in the CCS with the surge of anchovy during a warm period (Thompson et al., 2019) including an extremely high recruitment in 2016, preceded by one of the warmest years on records, represent good opportunities to identify model strengths and weaknesses. The multiple speculations on how EBUS and their fisheries might change over the next decades will hopefully motivate more active data acquisition, which will in turn help better assess model skills, increase biological realism, and ultimately enable model formulations that produce sufficiently reliable future projections of anchovy and sardine, and other species, under climate change.

Acknowledgements

This work was supported by the grant UMA18-FEDERJA-093 (FEDER program 2014-2020), from the Junta de Andalucía Spanish regional administration. We would like to thank Howard Townsend, Andrew Thompson, and two anonymous reviewers whose comments greatly helped improve our manuscript. The authors thankfully acknowledge supercomputing resources and technical support provided by the SCBI center of the University of Málaga.

Conflict of interest

The authors have no conflict of interest to declare.

Author contribution

J. C. Sánchez-Garrido and F. E. Werner conceived the original idea. K. A. Rose, J. Fiechter, and E. N. Curchitser designed the model and the computational framework. J. C. Sánchez-Garrido and J. Fiechter conducted the historical run and analyzed the data. All authors interpreted and discussed the results. J. C. Sánchez-Garrido wrote the paper with inputs from all authors.

Data availability statement

The model code and model output that generated the figures in the paper are available upon request to the corresponding author.

References

Alexander, M. A., Kilbourne, K. H., & Nye, J. A. (2014). Climate variability during warm and cold phases of the Atlantic Multidecadal Oscillation (AMO) 1871–2008. *Journal of Marine Systems*, **133**, 14–26.

Alheit, J., Roy, C., & Kifani, S. (2009). Decadal-scale variability in populations. In Checkley, D., Alheit, J., Oozeki, Y., Roy, C. (Eds.), Climate Change and Small Pelagic Fish. Cambridge University Press, New York, (pp. 64–87).

Alheit, J., & Ñiquen, M. (2004). Regime shifts in the Humboldt Current ecosystem. *Progress in Oceanography*, **60**, 201–222.

Alheit, J., Licandro, P., Coombs, S., García, A., Giráldez, A., García Santamaría, M. T., Slotte, A., & Tsikliras, A. C. (2014). Atlantic Multidecadal Oscillation (AMO) modulates dynamics of small pelagic fishes and ecosystem regime shifts in the eastern North and Central Atlantic. *Journal of Marine Systems*, **131**, 21–35.

Amante, C., & Eakins, B. W. (2009). ETOPO1 Arc-Minute Global Relief Model: Procedures, Data Sources and Analysis. NOAA Technical Memorandum NESDIS NGDC-24. National Geophysical Data Center, NOAA. doi:10.7289/V5C8276M.

Arístegui, J., Álvarez-Salgado, X. A., Barton, E. D., Figueiras, F. G., Hernández-León, S., Roy, C., & Santos, A. M. P. (2006). Oceanography and fisheries of the Canary Current Iberian region of the Eastern North Atlantic. In Robinson, A., Brink, K.H. (Eds.), The Global Coastal Ocean: Interdisciplinary Regional Studies and Syntheses, The Sea: Ideas and Observations on Progress in the Study of the Seas, vol. 14. Harvard University Press, pp. 877–931.

Arístegui, J., Barton, E. D., Álvarez-Salgado, X. A., Santos, A. M., Figueiras, F. G., Kifani, S., Hernández-León, S., Mason, E., Machú, E., & Demarcq, H. (2009). Sub-regional ecosystem variability in the Canary Current upwelling. *Progress in Oceanography*, **83**, 33–48.

Bakun, A. (1990). Global climate change and intensification of coastal ocean upwelling. *Science*, **247**, 198–201.

Braham, C. B. & Corten, A. (2015). Pelagic fish stocks and their response to fisheries and environmental variation in the Canary Current Large Marine Ecosystem. In: Oceanographic and biological features in the Canary Current Large Marine Ecosystem. Valdés, L. and Déniz-González, I. (eds). IOC UNESCO, Paris. IOC Technical Series, No. 115, pp. 197–213. URI: http://hdl.handle.net/1834/9189.

Brochier, T., Mason, E., Moyano, M., Berraho, A., Colas, F., Sangrà, P., Hernández-León, S., Ettahiri, O., & Lett, C. (2011). Ichthyoplankton transport from the African coast to the Canary Islands. *Journal of Marine Systems*, **87**(2), 109–122.

Brochier, T., Auger, P. -A. Pecquerie, L., Machu, E., Capet, X., Thiaw, M., Mbaye, B.C., Cheikh-Baye, B., Omar, E., Charouki, N., Sene, O. N., Werner, F., & Brehmer, P. (2018). Complex small pelagic fish population patterns arising from individual behavioral responses to their environment. *Progress in Oceanography*, 164:12-27. https://doi.org/10.1016/j.pocean.2018.03.011

Carton, J. A., & Giese, B. S. (2008). A reanalysis of ocean climate using Simple Ocean Data Assimilation (SODA). *Monthly Weather Review*, **136**, 2999–3017.

Chavez, F. P., Ryan, J., Lluch-Cota, S. E., & Ñiquen, M. (2003). From anchovies to sardines and back: multidecadal change in the Pacific Ocean. *Science*, **299**, 217–221.

Checkley, D., Asch, R. G., & Rykaczewski, R. R. (2017). Climate, Anchovy, and Sardine. *Annual Review of Marine Science*, **9**, 469–493.

Conkright, M. E., & Boyer, T. P. (2002). World Ocean Atlas 2001: Objective Analyses, Data Statistics, and Figures. CD-ROM Documentation, National Oceanographic Data Center, Silver Spring, MD, 17 pp.

FAO (2001). Report of the FAO working group on the assesment of small pelagic fish off Northwest Africa. FAO Fisheries Report No. 657, p. 133.

FAO (2012). Report of the FAO working group on the assesment of small pelagic fish off Northwest Africa. FAO Fisheries Report No. 1036, p. 245.

FAO (2019). FAO yearbook. Fishery and Aquaculture Statistics 2017/FAO annuaire. Statistiques des pêches et de l'aquiculture 2017/FAO anuario. Estadística de pesca y acuicultura 2017. Rome/Roma.

Fiechter, J., Kenneth A. R, Curchitser, E. N., & Hedstrom, K. S. (2015a). The role of environmental controls in determining sardine and anchovy population cycles in the California Current: Analysis of an end-to-end model. *Progress in Oceanography*, **138**, 381–398.

Fiechter, J., Huff, D. D., Martin, B. T., Jackson, D. W., Edwards, C. A., Rose, K. A., Curchitser, E. N., Hedstrom, K. S., Lindley, S. T., & Wells, B. K. (2015b). Environmental conditions impacting juvenile Chinook salmon growth off central California: An ecosystem model analysis. *Geophysical Research Letters*, **42**, 2910-2917.

Fiechter, J., Huckstadt, L. A., Rose, K. A., & Costa, D. P. (2016). A fully coupled ecosystem model to predict the foraging ecology of apex predators in the California Current. *Marine Ecology Progress Series*, **556**, 273-285.

Fulton, E. A. (2010). Approaches to end-to-end ecosystem models. *Journal of Marine Systems*, **81**(1–2), 171–183.

Humston, R., Olson, D. B., & Ault, J. S. (2004). Behavioral assumptions in models of fish movement and their influence on population dynamics. *Transactions of the American Fisheries Society*, **133**(6),1304–1328.

Hurrell, J. W. (1995). Decadal Trends in the North Atlantic Oscillation: Regional Temperatures and Precipitation. *Science*, **269**, 676-679.

Kalnay, E., Kanamitsu, M., Kistler, R., Collins, W., Deaven, D., Gandin, L., Iredell, M., Saha, S., White, G., Woollen, J., Zhu, Y., Chelliah, M., Ebisuzaki, W., Higgins, W., Janowiak, J., Mo, K.C., Ropelewski, C., Wang, J., Leetmaa, A., Reynolds, R., Jenne, R., & Joseph, D. (1996). The NCEP/NCAR 40-Year Reanalysis Project. *Bulletin of the American Meteorological Society*, **77**, 437–472.

Kishi, M. J., Kashiwai, M., Ware, D. M., Megrey, B. A., Eslinger, D. L., Werner, F. E., Aita-Noguchi, M., Azumaya, T., Fujii, M., Hashimoto, S., Huang, D., Iizumi, H., Ishida, Y., Kang, S., Kantakov, G.A., Kim, H. - C., Komatsu, K., Navrotsky, V.V., Smith, L.S., Tadokoro, K., Tsuda, A., Yamamura, O., Yamanaka, Y., Yokouchi, K., Yoshie, N., Zhang, J., Zuenko, Y. I., & Zvansky, V. I. (2007). NEMURO – introduction to a lower trophic level model for the North Pacific marine ecosystem. *Ecological Modelling*, **202**, 12–25.

Kishi, M. J., Ito, S., Megrey, B. A., Rose, K. A., & Werner, F. E. (2011). A review of the NEMURO and NEMURO.FISH models and their application to marine ecosystem investigations. *Journal of Oceanography*, **67**, 3–16.

Large, W. G., McWilliams, J. C., & Doney, S. C. (1994). Oceanic vertical mixing: A review and a model with a vertical K-profile boundary layer parameterization. *Reviews of Geophysics*, **32**(4), 363–403.

Large, W. G., & Yeager, S. G. (2008). The global climatology of an interannually varying air–sea flux data set. *Climate Dynamics*, **33**, 341–363.

Lindegren, M., Checkley, D. M., Rouyer, T., MacCall, A. D., & Stenseth, N. C. (2013). Climate, fishing, and fluctuations of sardine and anchovy in the California Current. Proceedings of the National Academy of *Sciences*, **110** (33), 13672–13677.

Lluch-Cota, S.E. (2013). Modeling sardine and anchovy low-frequency variability. *Proceedings of the National Academy of Sciences*, **110**(33), 13240–13241.

López-Parages, J., Auger, P.-A., Rodríguez-Fonseca, B., Keenlyside, N., Gaetan, C., Rubino, A., Woldeyes Arisido, M., & Brochier, T. (2020). El Niño as a predictor of round sardinella distribution along the northwest African coast. *Progress in Oceanography*, **186**, 102341.

Marshall, J., Kushner, Y., Battisti, D., Chang, P., Czaja, A., Dickson, R., Hurrell, J., McCartney, M., Saravanan, R., & Visbeck, M. (2001). North Atlantic climate variability: phenomena, impacts and mechanisms. *International Journal of Climatology*, **21**, 1863–1898.

McClatchie, S., Hendy, I. L., Thompson, A. R., & Watson, W. (2017). Collapse and recovery of forage fish populations prior to commercial exploitation. *Geophysical Research Letters*, **44**, 1877-1885.

Nishikawa, H., Curchitser, E. N., Fiechter, J., Rose, K. A. & Hedstrom, K. (2019). Using a climate-to-fishery model to simulate the influence of the 1976–1977 regime shift on anchovy and sardine in the California Current System. *Progress in Earth and Planetary Science*, **6**, 9 https://doi.org/10.1186/s40645-019-0257-2

Oozeki, Y., Ñiquen Carranza, M., Takasuka, A., Ayón Dejo, P., Kuroda, H., Tam Malagas, J., Okunishi, T., Vásquez Espinoza, L., Gutiérrez Aguilar, D., Okamura, H., & Guevara Carrasco, R. (2019). Synchronous multi-species alternations between the northern Humboldt and Kuroshio Current systems. *Deep Sea Research Part II*, **159**, 11–21.

Politikos, D. V., Curchitser, E. N., Rose, K. A., Checkley, D. M & Fiechter, J. (2018). Climate variability and sardine recruitment in the California Current: A mechanistic analysis of an ecosystem model. *Fisheries Oceanography*, **27**, 602–622, DOI: 10.1111/fog.12381.

Rose, K.A. (2000). Why are quantitative relationships between environmental quality and fish populations so elusive? *Ecological Applications*, **10**, 367-385.

Rose, K. A., Allen, J. I., Artioli, Y., Barange, M., Blackford, J., Carlotti, F., Cropp, R., Daewel, U., Edwards, K., Flynn, K., Hill, S. L., HilleRisLambers, R., Huse, G., Mackinson, S., Megrey, B., Moll, A., Rivkin, R., Salihoglu, B., Schrum, C., Shannon, L., Shin, Y. -J., Smith, S. L., Smith, C., Solidoro, C., St. John, M., & Zhou, M. (2010). End-to-end models for the analysis of marine ecosystems: challenges, issues, and next steps. *Marine and Coastal Fisheries*, **2**, 115–130.

Rose, K. A. , Fiechter, J., Curchitser, E. N., Hedstrom, K., Bernal, M., Creekmore, S., Haynie, A., Ito, S., Lluch-Cota, S., Megrey, B.A., Edwards, C. A., Checkley, D., Koslow, T., McClatchie, S., Werner, F., MacCall, A., & Agostini, V. (2015). Demonstration of a fully-coupled end-to-end model for small pelagic fish using sardine and anchovy in the California Current. *Progress in Oceanography*, **138**, 348–380.

Sánchez-Garrido, J. C., Werner, F. E., Fiechter, J., Rose, K. A., Curchitser, E. N., Ramos, A., García Lafuente, J., Arístegui, J., Hernández-León, S., & Rodríguez Santana, A. (2019). Decadal-scale variability of sardine and anchovy simulated with an end-to-end coupled model of the Canary Current ecosystem. *Progress in Oceanography*, **171**, 212–230.

Scheffer, M., Baveco, J. M., De Angelis, D. L., Rose, K. A., & van Nes, E. H. (1995). Super-individuals a simple solution for modelling large populations on an individual basis. *Ecological Modelling*, **80**, 161–170.

Schwartzlose, R. A., Alheit, J., Bakun, A., Baumgartner, T., Cloete, R., Crawford, R. J .M., Fletcher, W. J., Green-Ruíz, Y., Hagen, E., Kawasaki, T., Lluch-Belda, D., Lluch- Cota, S. E., MacCall, A. D., Matsuura, Y., Nevarez-Martinez, M. O., Parrish, R. H., Roy, C., Serra, R., Shust, K. V., Ward, N. M., & Zuzunaga, J. Z.

(1999). Worldwide large-scale fluctuations of sardine and anchovy populations. *South African Journal of Marine Sciences*, **21**, 289–347.

Sera, R., & Tsukayama, I. (1998). Sinopsis de datos biológicos y pesqueros de la sardina, Sardinops sagax en el Pacífico suroriental. FAO. Sinop. Pesca, (13) Rev,1:60p.

Shchepetkin, A. F., & McWilliams, J. C. (2005). The regional oceanic modeling system (ROMS): a split-explicit, free-surface, topography-following-coordinate oceanic model. *Ocean Modelling*, **9**, 347–404.

Takasuka, A., Oozeki, Y., Kubota, H., & Lluch-Cota, S. E. (2008). Contrasting spawning temperature optima: Why are anchovy and sardine regime shifts synchronous across the North Pacific? *Progress in Oceanography*, **77**, 225–232.

Thiaw, M., Auger, P. A., Ngom, F., Brochier, T., Faye, S., Diankha, O., & Brehmer, P. (2017). Effect of environmental conditions on the seasonal and inter-annual variability of small pelagic fish abundance off North-West Africa: the case of both Senegalese sardinella. *Fisheries Oceanography*, **26**, 583-601.

Thompson, A., Schroeder, I., Bograd, S., Hazen, E., Jacox, M., Leising, A., Wells, B., Largier, J., Fisher, J., Jacobson, K., Zeman, S., Bjorkstedt, E., Robertson, R., Kahru, M., Goericke, R., Peabody, C., Baumgartner, T., Lavaniegos, B., Miranda, L., & Melin, S. (2019). State of the California Current 2018-2019: a novel anchovy regime and a new marine heatwave?

Trenberth, K. E., & Shea, D. J. (2006). Atlantic hurricanes and natural variability in 2005, *Geophysical Research Letters*, **33**, L12704

Visbeck. M., Cullen, H., Krahmann, G., & Naik., N. (1998). An ocean model's response to North Atlantic Oscillation-like wind forcing. *Geophysics Research Letters*, **25**, 4521–4524.

Watkins, K. S., & Rose, K. A. (2013). Evaluating the performance of individual-based animal movement models in novel environments. *Ecological Modelling*, **250**, 214–234.

Werner, F. E., Ito, S., Megrey, B. A., Michio, J., & Kishi, M. J. (2007). Synthesis of the NEMURO model studies and future directions of marine ecosystem modelling. *Ecological Modelling*, **202**, 211–223.

Zwolinski, J., & Demer, D. (2012), A cold oceanographic regime with high exploitation rates in the northeast Pacific forecasts a collapse of the sardine stock, *Proceedings of National Academy of Science of the United States of America*, **109**(11), 4175–4180, doi:10.1073/pnas.1113806109.

Figure captions

Figure 1: Model grid and bathymetry. For clarity, only 1 of every 3 grid lines is shown. Labels stand for Gulf of Cádiz (GoC), Cape Ghir (CG), Cape Juby (CJ), and Cape Blanc (CB).

Figure 2: Mean anchovy and sardine abundance maps during the simulated period 1964-2008. Abundance is given in $\log_{10}$ (number of individuals) and for different life stages. From left to right: eggs + yolk-sacs, larvae, juveniles, and adults (age-1 and older). For each horizontal grid cell, mean abundance was calculated as the sum of the total number of individuals within that cell over all model outputs (one output every 5 days), divided by the total number of outputs.

Figure 3: Adult (age-1 and older) anchovy and sardine abundance anomaly on January 1 each year. Anomalies are with respect to the 1964-2008 mean and standardized.

Figure 4: Adult (age-1 and older) worth versus age-0 survival fraction (upper panels) and yearly egg production (bottom panels). Adult worth is for the current year; survival fraction and egg production are for the year prior.

Figure 5: Age-0 survival versus egg+yolk-sac larva (EYS), larva (Lrv), and juvenile (Juv) survival fractions.

Figure 6: Adult worth versus age-1, age-2, age-3, and age-4 egg production. Adult worth is for the current year; number of eggs is for the year prior.

Figure 7: Sardine age-2 fecundity (number of eggs per individual) versus age-2 egg production (top left), age-1 weight the year prior (top right), age-1 growth the year prior (bottom left), and age-2 growth the same year (bottom right).

Figure 8: Anchovy age-0 survival (top) and sardine age-1 growth (bottom) annual anomalies. Anomalies are with respect to the 1964-2008 mean and standardized. Years labeled in red and blue colors correspond to years with anomalies lying one standard deviation above and

below the mean, respectively, and are defined as good (red) and bad (blue) years. The rest of the years are referred to as normal years.

Figure 9: Mean temperature (ºC) and prey availability (*P*) experienced by anchovy early life stages during normal years (central panels). Side panels: anomalies with respect to normal conditions during good (right) and bad (left) years (high and low age-0 survival, respectively). Top panels are for eggs and yolk-sac larvae; middle and bottom panels are for larvae.

Figure 10: Mean temperature (ºC) and prey availability (*P*) experienced by sardine age-1 during normal years (central panels). Side panels: anomalies with respect to normal conditions during good (right) and bad (left) years (high and low age-1 growth, respectively).

Figure 11: From left to right: SST (ºC), total surface phytoplankton (mmol Nm^{-3}), total surface zooplankton (mmol N m^{-3}), and along-shore northern wind stress component (× 10 Nm^{-2}) anomaly during years of high (top) and low (bottom) anchovy age-0 survival. Anomalies are derived from ROMS and NEMURO and correspond to deviations with respect to the 1964-2008 mean.

Figure 12: From left to right: SST (ºC), total surface phytoplankton (mmol N m^{-3}), total surface zooplankton (mmol N m^{-3}), and along-shore northern wind stress component (× 10 Nm^{-2}) anomaly during years of high (top) and low (bottom) sardine age-1 growth. Anomalies are derived from ROMS and NEMURO and correspond to deviations with respect to the 1964-2008 mean.

Figure 13: First three EOF modes for SST (upper row), total surface phytoplankton (middle), and total surface zooplankton (bottom) from annual series of ROMS and NEMURO. The percentage of the total variance explained by each mode is labeled. The normalized temporal amplitudes are shown in the right panels.

Figure 14: Anchovy (left) and sardine (right) standardized annual abundance anomaly. Red and black lines indicate periods of clearly positive (>0.5 STD) and negative (<-0.5 STD) EOF

temporal amplitudes for SST (top), total surface phytoplankton (center), and total surface zooplankton (bottom).

Figure 15: Standardized annual series of the North Atlantic Oscillation index (NAO; source: www.esrl.noaa.gov, the Atlantic Multidecaldal Oscillation index (AMO; source: www.esrl.noaa.gov), the El Niño 3.4 index (ENSO; source: www.cpc.ncep.noaa.gov), and the Bakun Upwelling Index at 30ºN (UI30N; computed from the model wind forcing).

Figure 16: Anchovy age-0 survival (top) and sardine age-1 growth (bottom) anomaly versus climate indexes. From left to right: North Atlantic Oscillation (NAO), Atlantic Multidecadal Oscillation (AMO), El Niño 3.4 (ENSO), and Upwelling Index at 30ºN (UI30N). Only years of high and low anchovy age-0 survival and sardine age-1 growth are included. The solid line is the linear regression line. The Pearson correlation coefficient is labeled in each panel, with asterisk marks indicating significant correlation at a probability level of α=0.05.

Figure 17: Flow chart summarizing the main environmental and biological drivers for the variability of anchovy and sardine adult populations in the CanCS (left) and in the CCS (right; from Fiechter et al., 2015a).

Figure 18: Box plots of anchovy and sardine yearly attributes in the CanCS and the CCS. Left: temperature experienced by eggs and ysacs; center: egg and ysac development time; right: egg and ysac survival fraction. Central rectangles span the first quartil (Q1) to the third (Q3); segments inside boxes represent the median. The upper (lower) whisker extends to the first (last) datum smaller (greater) than Q3+1.5 × IQR (Q3-1.5 × IQR), where IQR=(Q3-Q1) is the interquartile range.

Table captions

Table 1: Pearson correlation coefficient for anchovy worth. Values in bold correspond to plotted curves (Figure 4). Underlined values indicate highest correlation coefficient over all lags.

Table 2: Pearson correlation coefficient for sardine worth. Values in bold correspond to plotted curves (Figure 4). Underlined values indicate highest correlation coefficient over all lags.

Table 3: Pearson correlation coefficient for sardine age-2 fecundity (annual egg production per age-2 individual). Values in bold correspond to plotted curves (Figure 7). Underlined values indicate highest correlation coefficient over all lags.

Table 4: Mean temperature and food abundance (P) experienced by anchovy larvae during normal, good, and bad years. Conditions during good and bad years are given as anomalies with respect to normal years. ΔC_T and ΔC_P denote percent variations with respect to normal consumption due to temperature and food anomalies, based on eq. (1).

Table 5: Mean temperature and food abundance (P) experienced by sardine age-1 during normal, good, and bad years. Conditions during good and bad years are given as anomalies with respect to normal years. ΔC_T and ΔC_P denote percent variations with respect to normal consumption due to temperature and food anomalies, based on eq. (1).

Table 6: Pearson correlation coefficient between climate indexes and EOF temporal amplitudes for annual SST (mode 1), total surface phytoplankton (mode 3), and total surface zooplankton (mode 1). Underlined values indicate highest correlation coefficient for each mode. Asterisk mark indicates significant correlation at a probability level of α=0.05.

Lag/Variables	-2 years	-1 year	0 year	+1 year
Adult Worth vs. Age-0 Survival	0.36	**0.43**	-0.11	-0.13
Adult Worth vs. Egg Production	0.54	**0.75**	0.86	0.90
Adult Worth vs. Age-1 Egg Prod.	0.10	**0.27**	0.34	-0.01
Adult Worth vs. Age-2 Egg Prod.	0.47	**0.62**	0.63	0.80
Adult Worth vs. Age-3 Egg Prod.	0.37	**0.55**	0.72	0.68
Adult Worth vs. Age-4 Egg Prod.	0.32	**0.44**	0.58	0.63

Table 1: Pearson correlation coefficient for anchovy worth. Values in bold correspond to plotted curves (Figure 4). Underlined values indicate highest correlation coefficient over all lags.

Lag/Variables	-2 years	-1 year	0 year	+1 year
Adult Worth vs. Age-0 Survival	-0.07	**0.01**	-0.40	-0.47
Adult Worth vs. Egg Production	0.66*	**0.75**	0.64	0.54
Adult Worth vs. Age-1 Egg Prod.	0.52*	**0.45**	0.26	-0.05
Adult Worth vs. Age-2 Egg Prod.	0.59*	**0.62**	0.53	0.42
Adult Worth vs. Age-3 Egg Prod.	0.55*	**0.61**	0.49	0.50
Adult Worth vs. Age-4 Egg Prod.	0.36*	**0.58**	0.57	0.50

Table 2: Pearson correlation coefficient for sardine worth. Values in bold correspond to plotted curves (Figure 4). Underlined values indicate highest correlation coefficient over all lags.

Lag/Variables	-2 years	-1 year	0 year	+1 year
Age-2 Eggs/Ind. vs. Age-2 Egg Prod.	-0.28	0.03	**0.45**	0.39
Age-2 Eggs/Ind. vs. Age-1 Weight	0.15	**0.23**	0.15	-0.13
Age-2 Eggs/Ind. vs. Age-1 Growth	0.23	**0.79**	0.39	0.02
Age-2 Eggs/Ind. vs. Age-2 Growth	0.12	0.59	**0.33**	-0.05

Table 3: Pearson correlation coefficient for sardine age-2 fecundity (anual egg production per age-2 individual). Values in bold correspond to plotted curves (Figure 7). Underlined values indicate highest correlation coefficient over all lags.

	Anchovy lrv.			
Years	Temp (°C)	ΔC_T	P	ΔC_P
Normal	19.14	-	0.837	-
Good	-0.13	-0.020%	+0.028	+3.5%
Bad	+0.22	+0.026%	-0.019	-2.3%

Table 4: Mean temperature and food abundance (P) experienced by anchovy larvae during normal, good, and bad years. Conditions during good and bad years are given as anomalies with respect to normal years. ΔC_T and ΔC_P denote percent variations with respect to normal consumption due to temperature and food anomalies, based on eq. (1).

Sardine age-1				
Years	Temp (°C)	ΔC_T	P	ΔC_P
Normal	21.16	-	0.714	-
Good	-0.31	+0.5%	+0.017	+2.4%
Bad	+0.45	-1.1%	-0.014	-2.0%

Table 5: Mean temperature and food abundance (P) experienced by sardine age-1 during normal, good, and bad years. Conditions during good and bad years are given as anomalies with respect to normal years. ΔC_T and ΔC_P denote percent variations with respect to normal consumption due to temperature and food anomalies, based on eq. (1).

EOF mode	NAO	AMO	ENSO	UI30N
Temp. Mode 1	-0.49*	0.59*	0.12	-0.35*
Phyt. Mode 3	-0.44*	0.52*	0.31*	-0.17
Zoop. Mode 1	-0.27	0.04	0.37*	-0.54*

Table 6: Pearson correlation coefficient between climate indexes and EOF temporal amplitudes for annual SST (mode 1), total surface phytoplankton (mode 3), and total surface zooplankton (mode 1). Underlined values indicate highest correlation coefficient for each mode. Asterisk mark indicates signifficant correlation at a probability level of α=0.05.

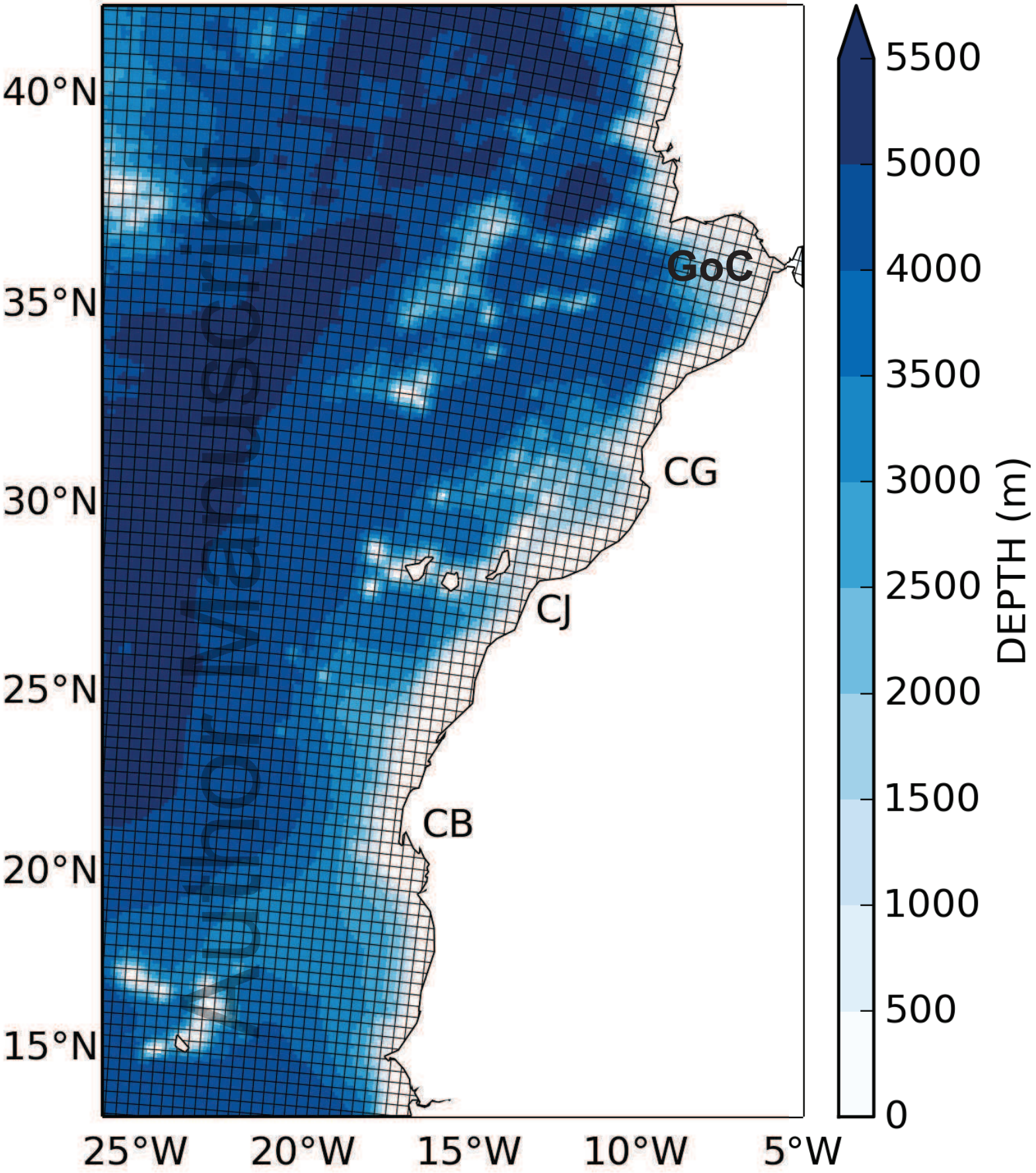

fog_12516_f1.eps

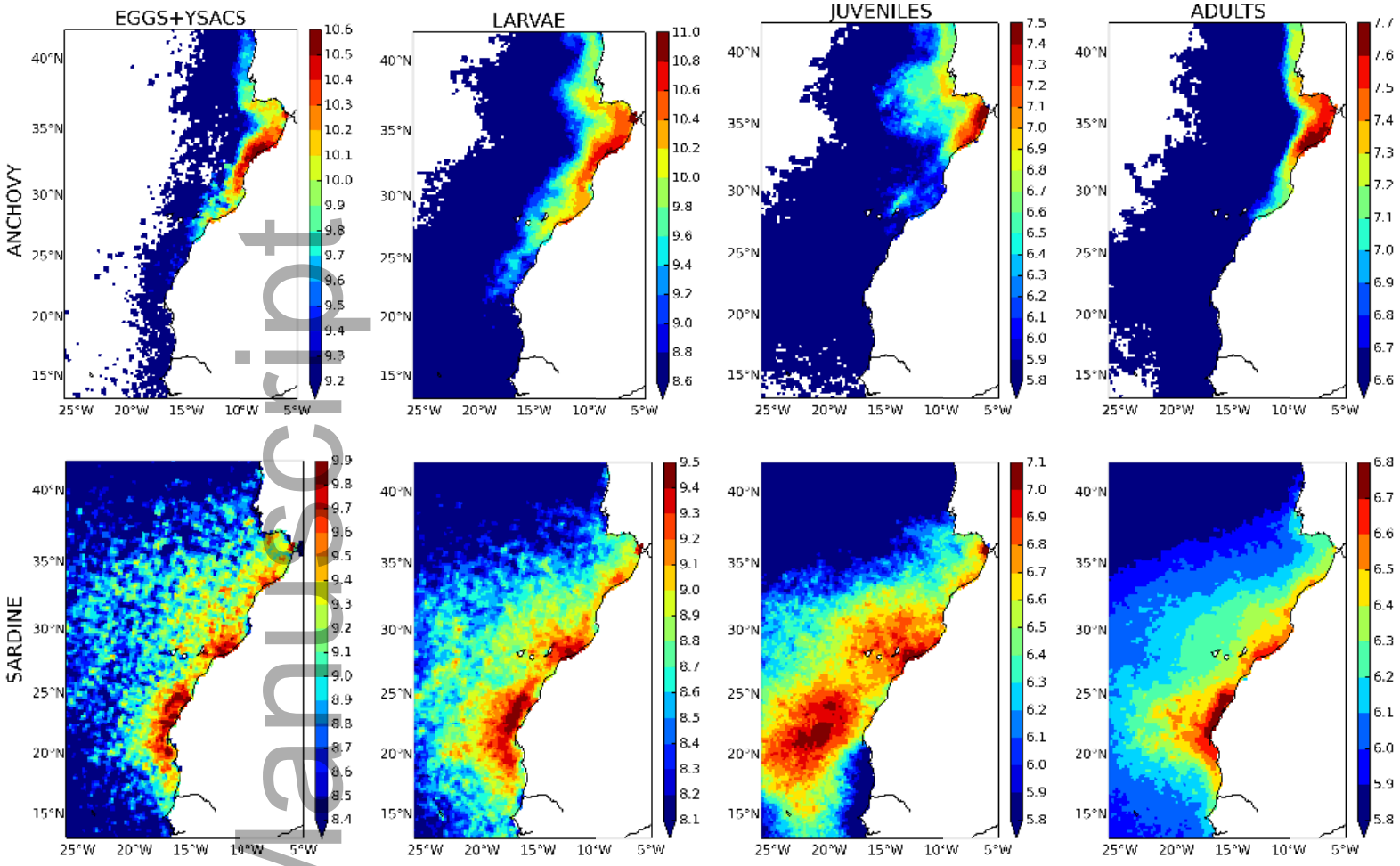

fog_12516_f2.eps

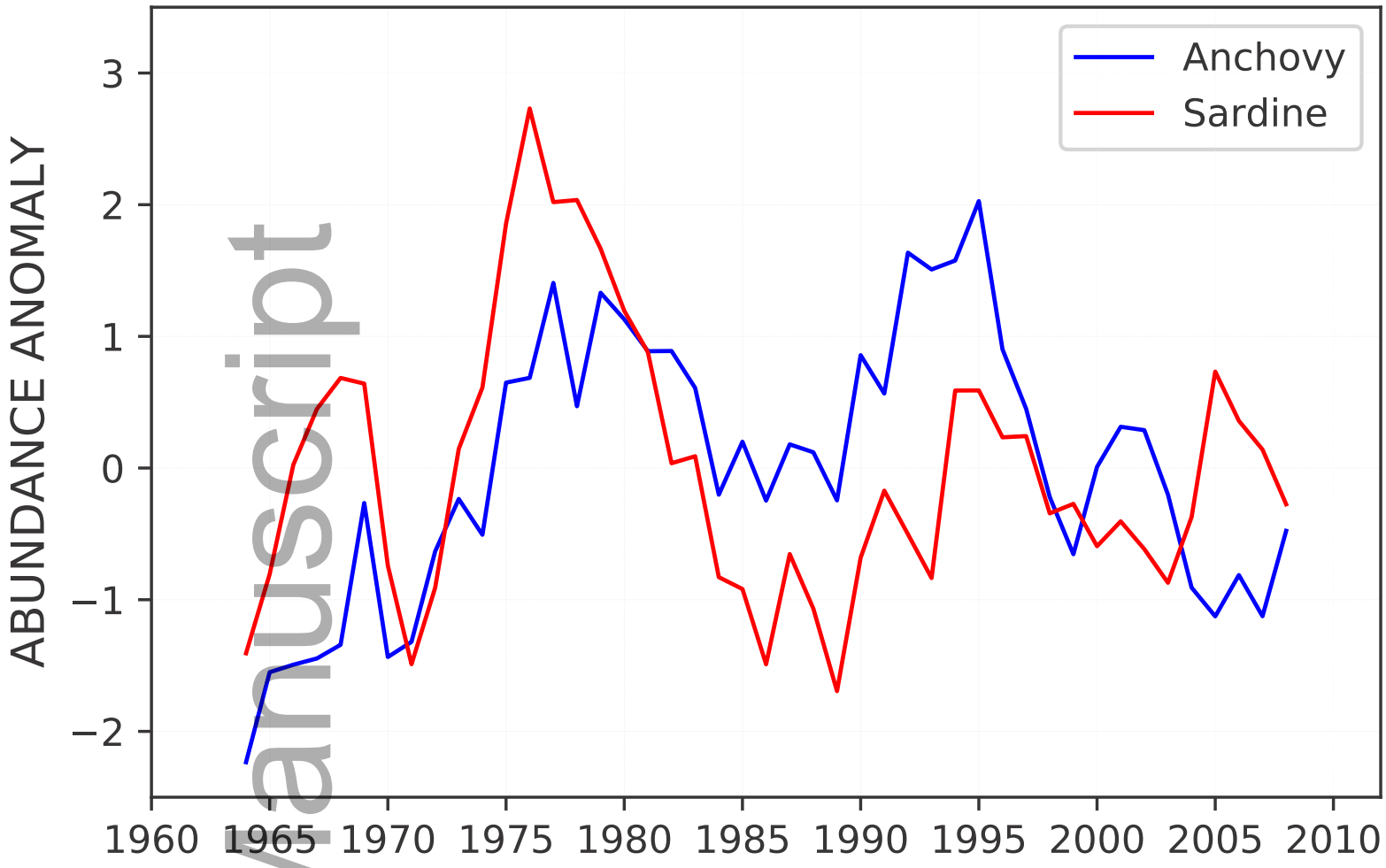

fog_12516_f3.eps

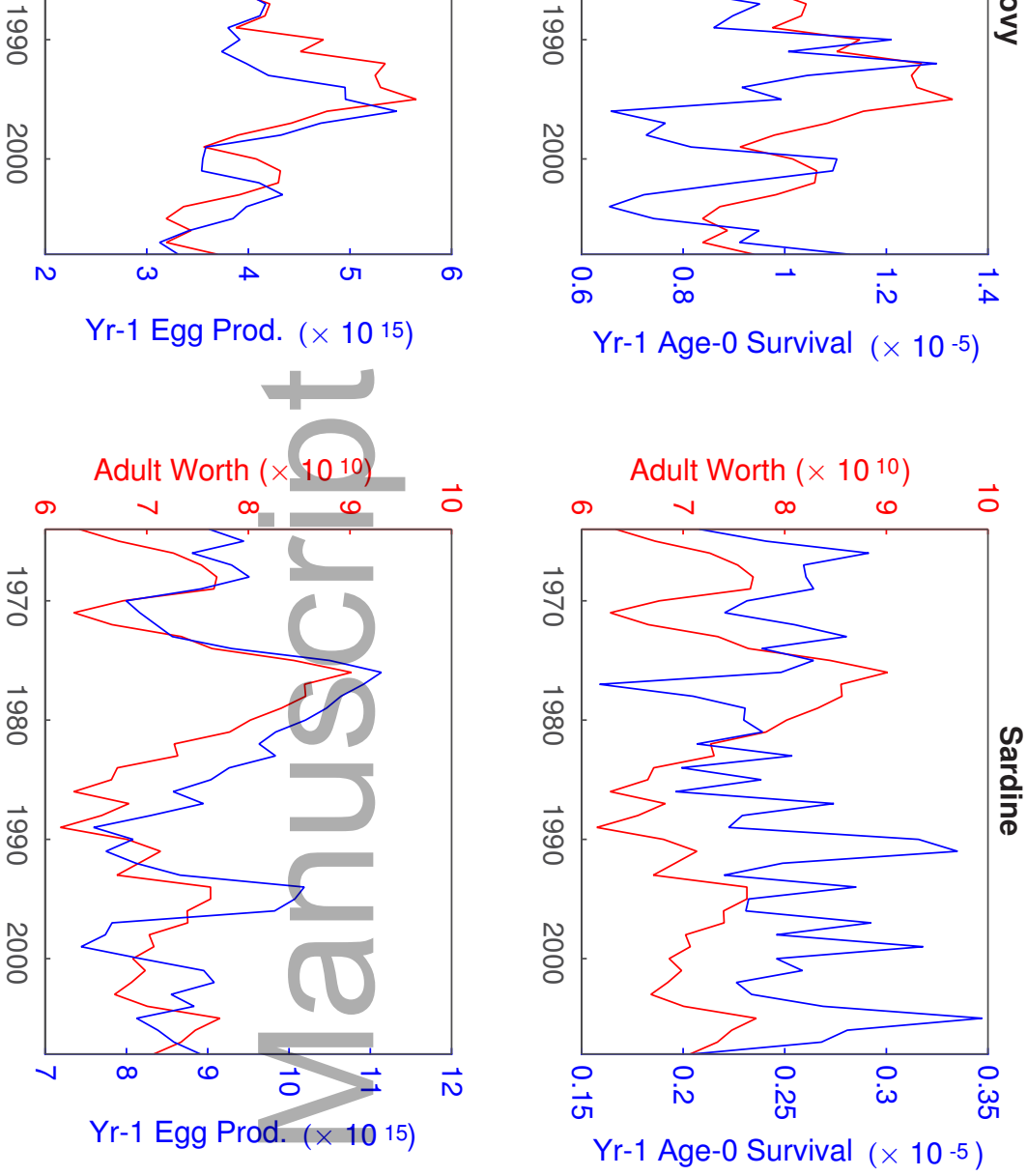

fog_12516_f4.eps

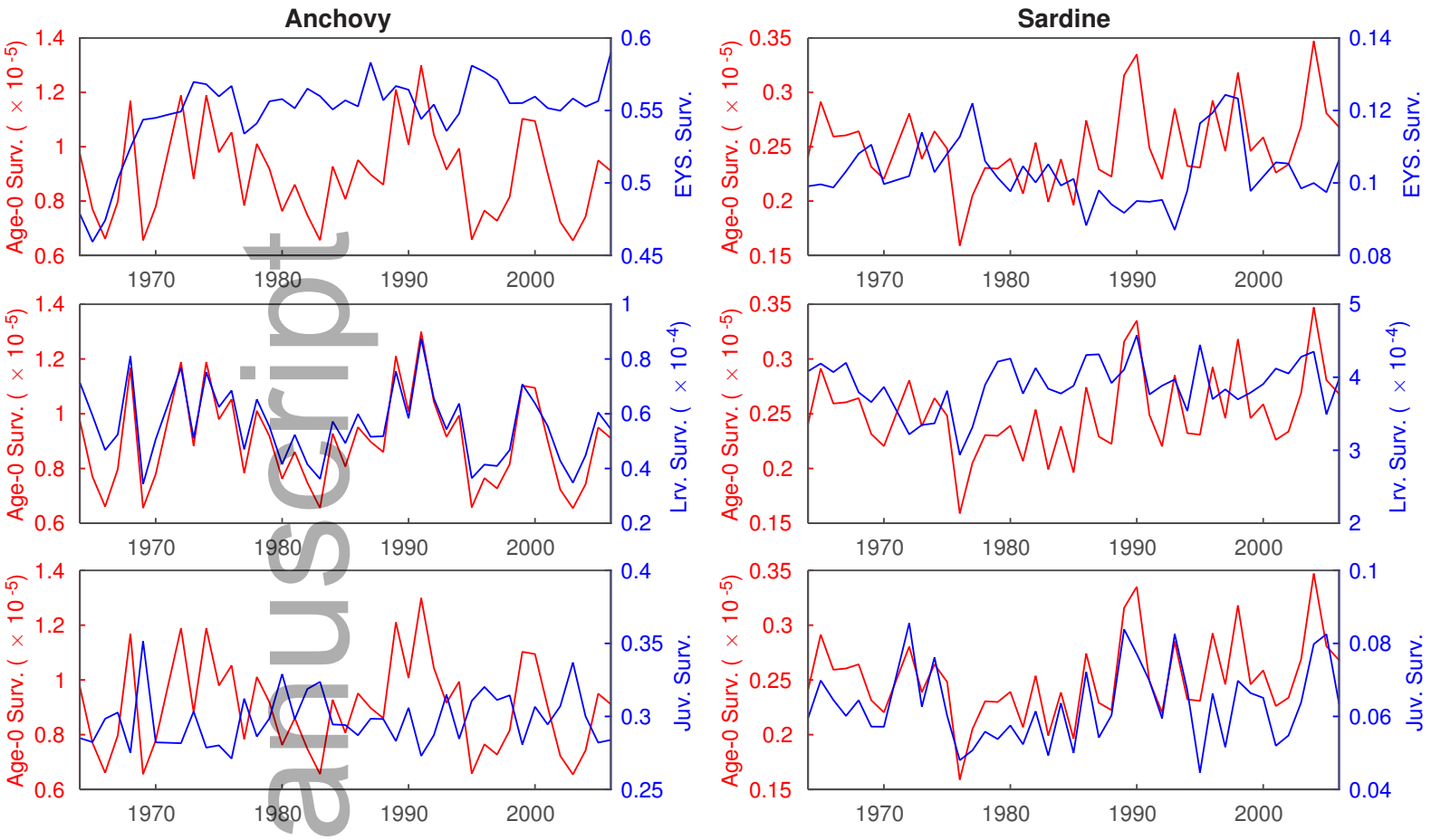

fog_12516_f5.eps

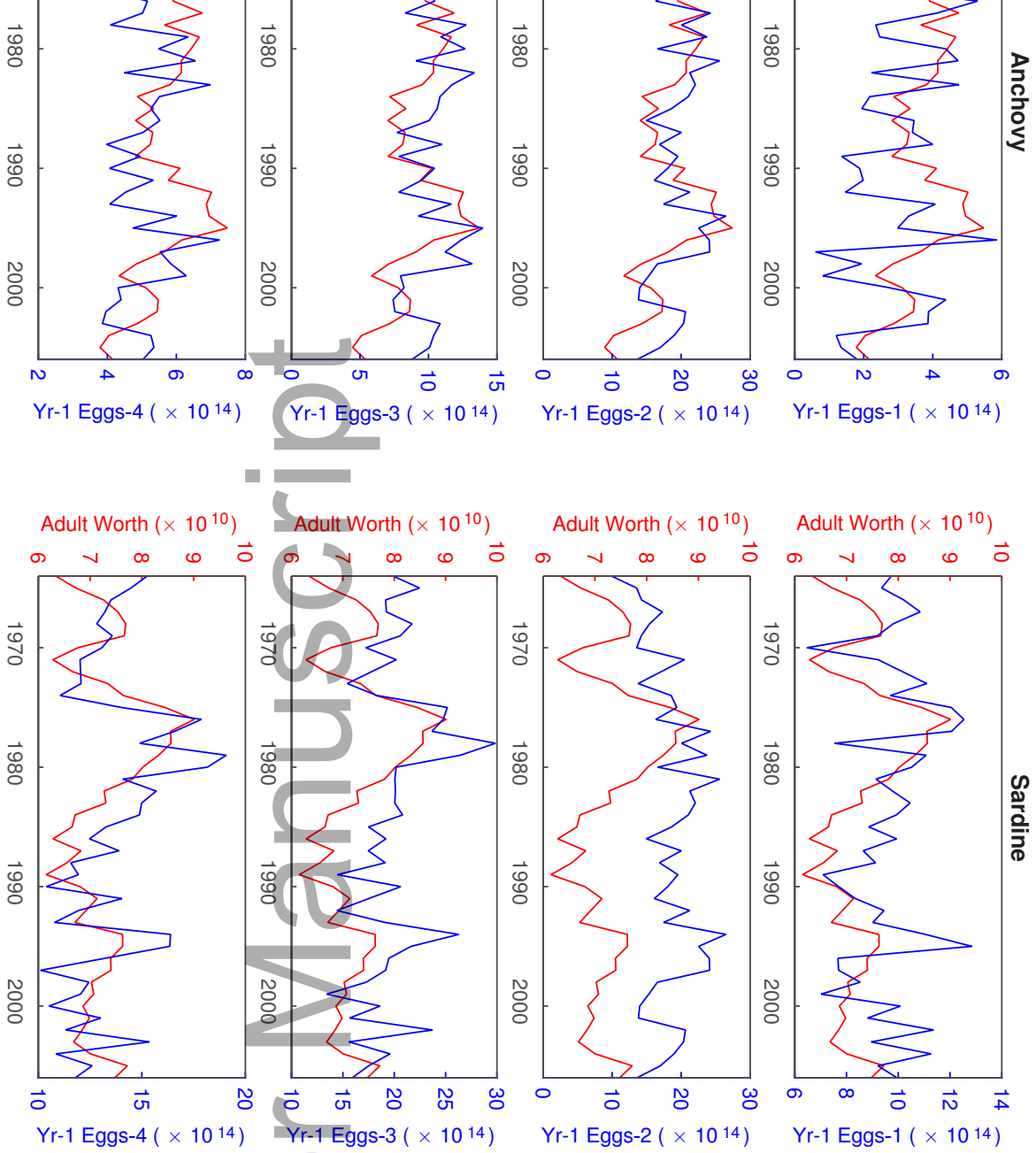

fog_12516_f6.eps

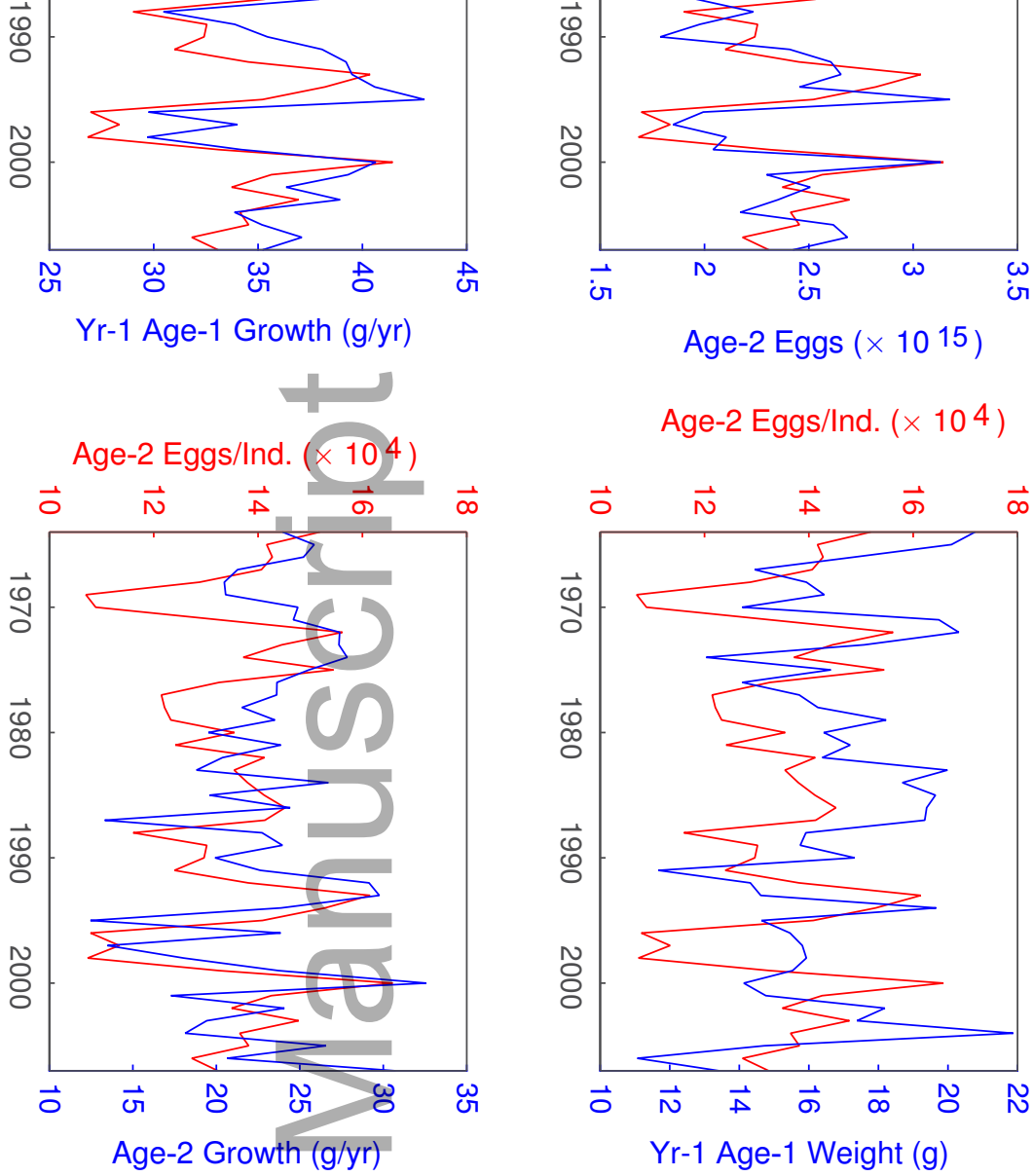

fog_12516_f7.eps

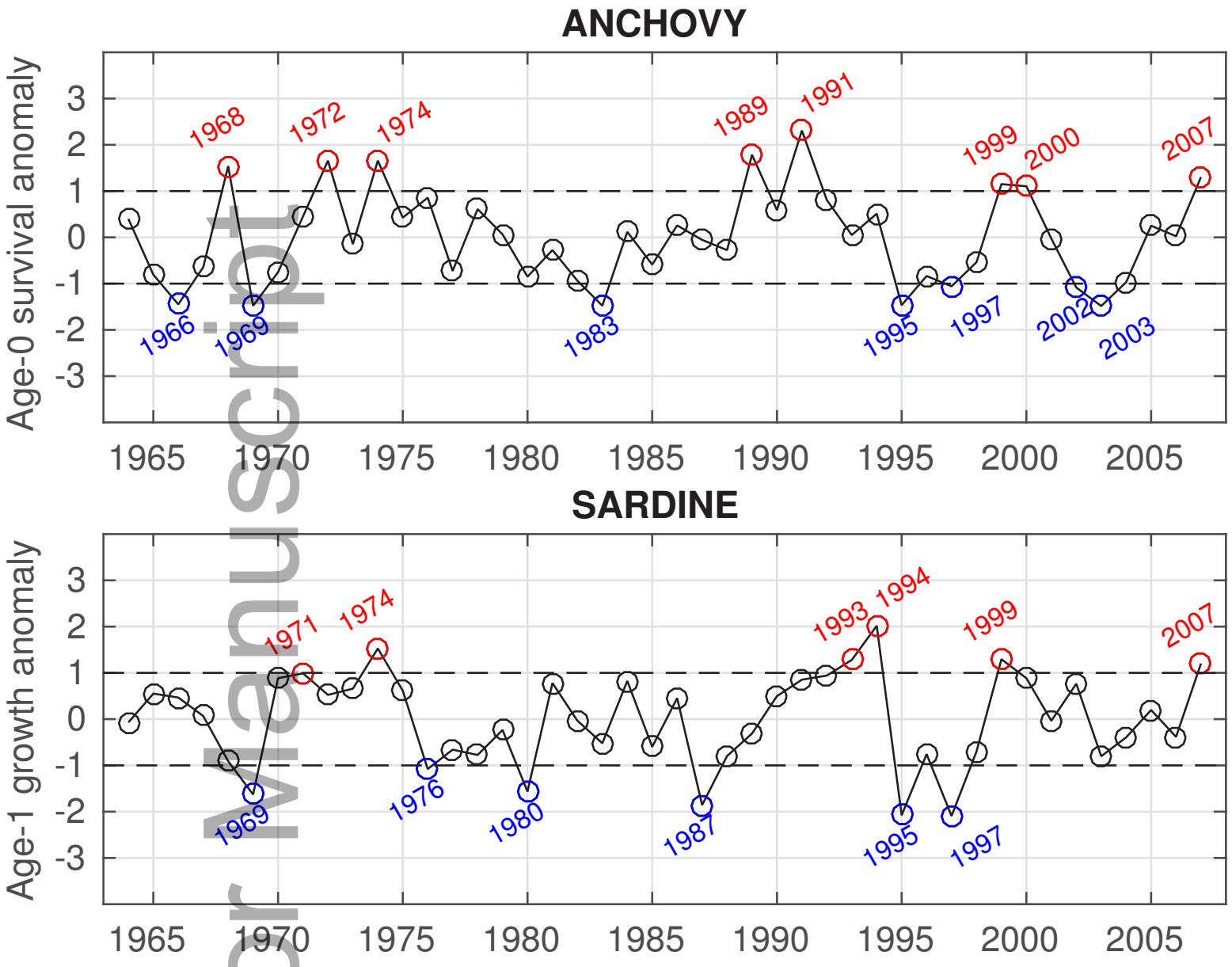

fog_12516_f8.eps

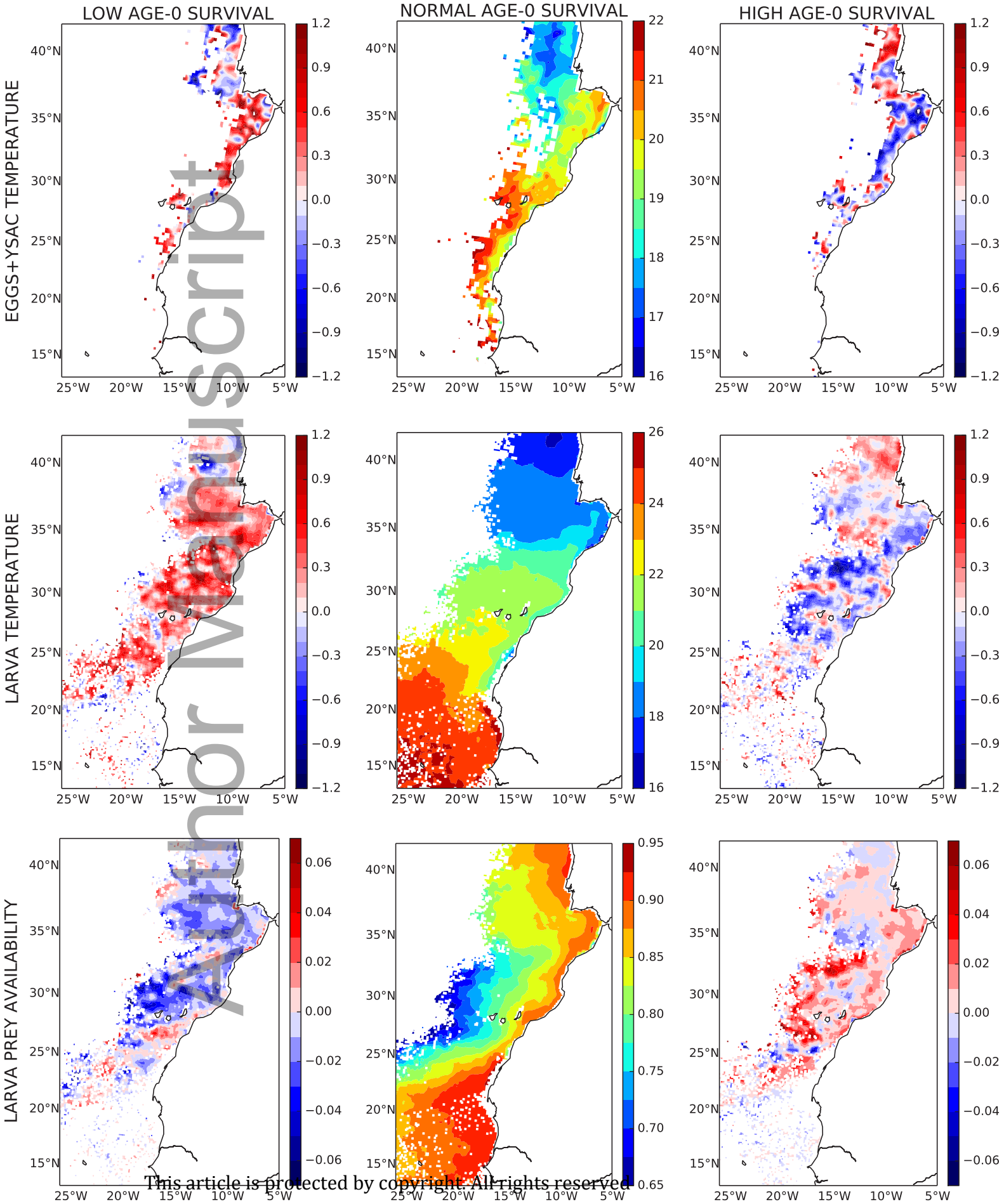

fog_12516_f9.eps

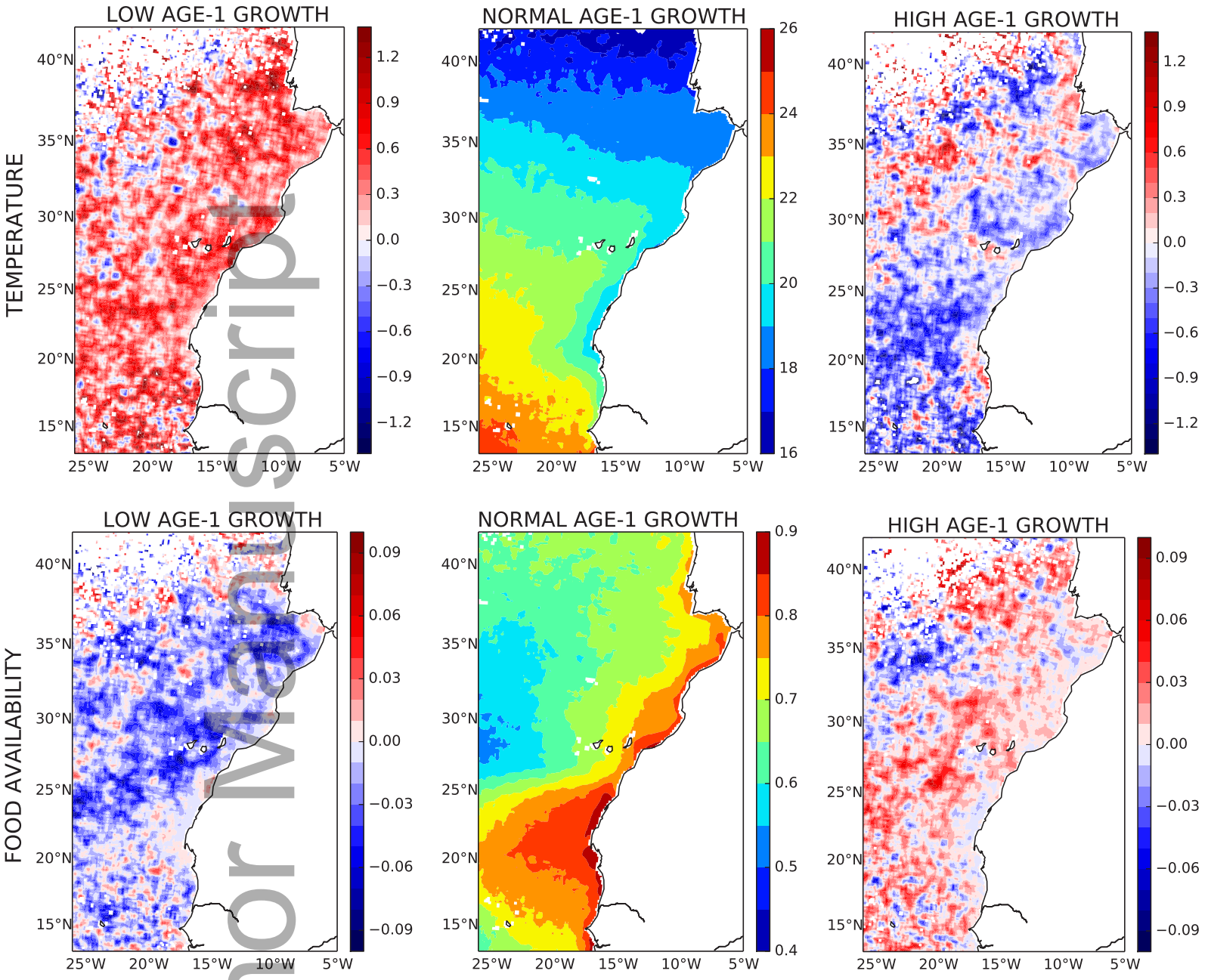

fog_12516_f10.eps

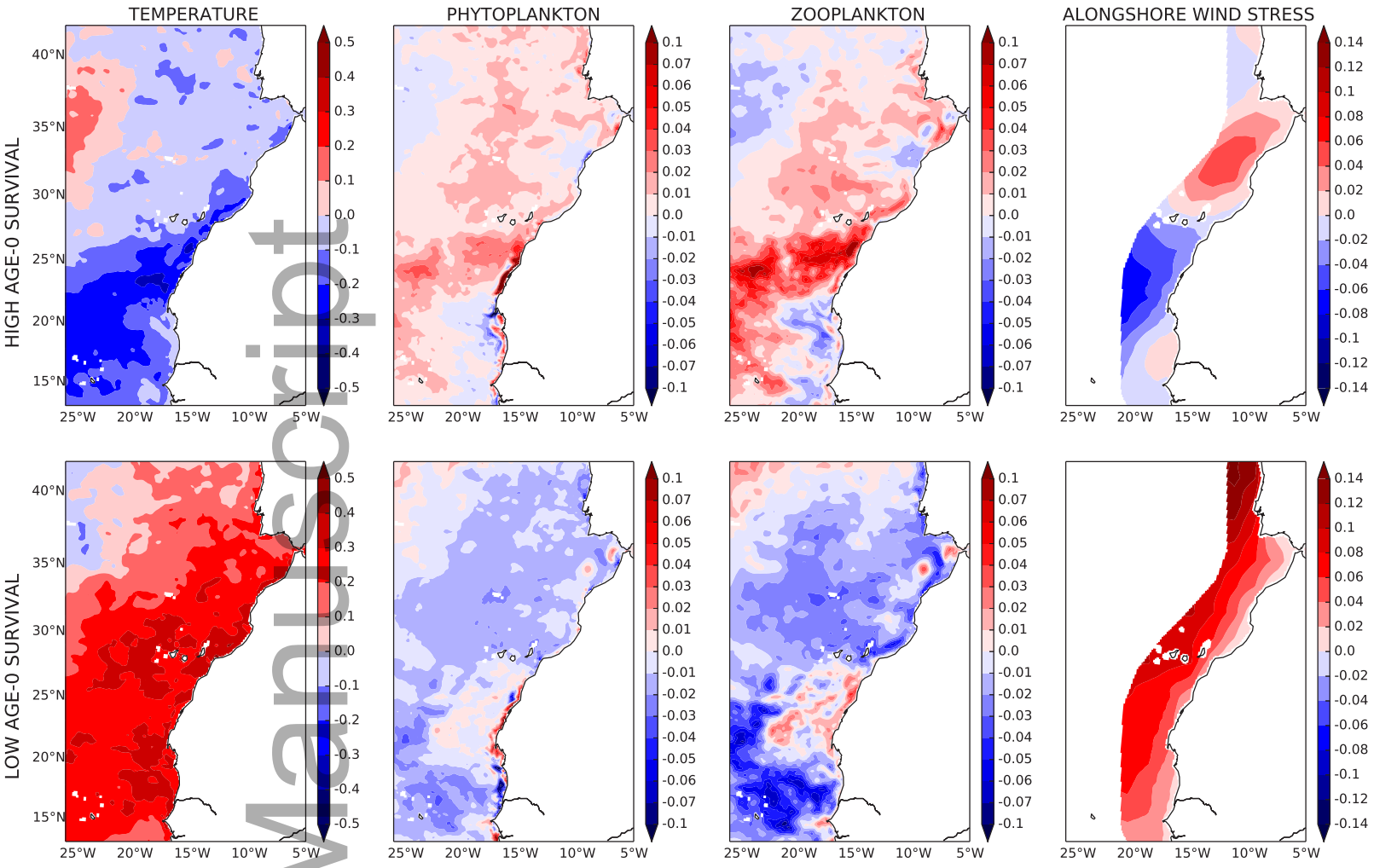

fog_12516_f11.eps

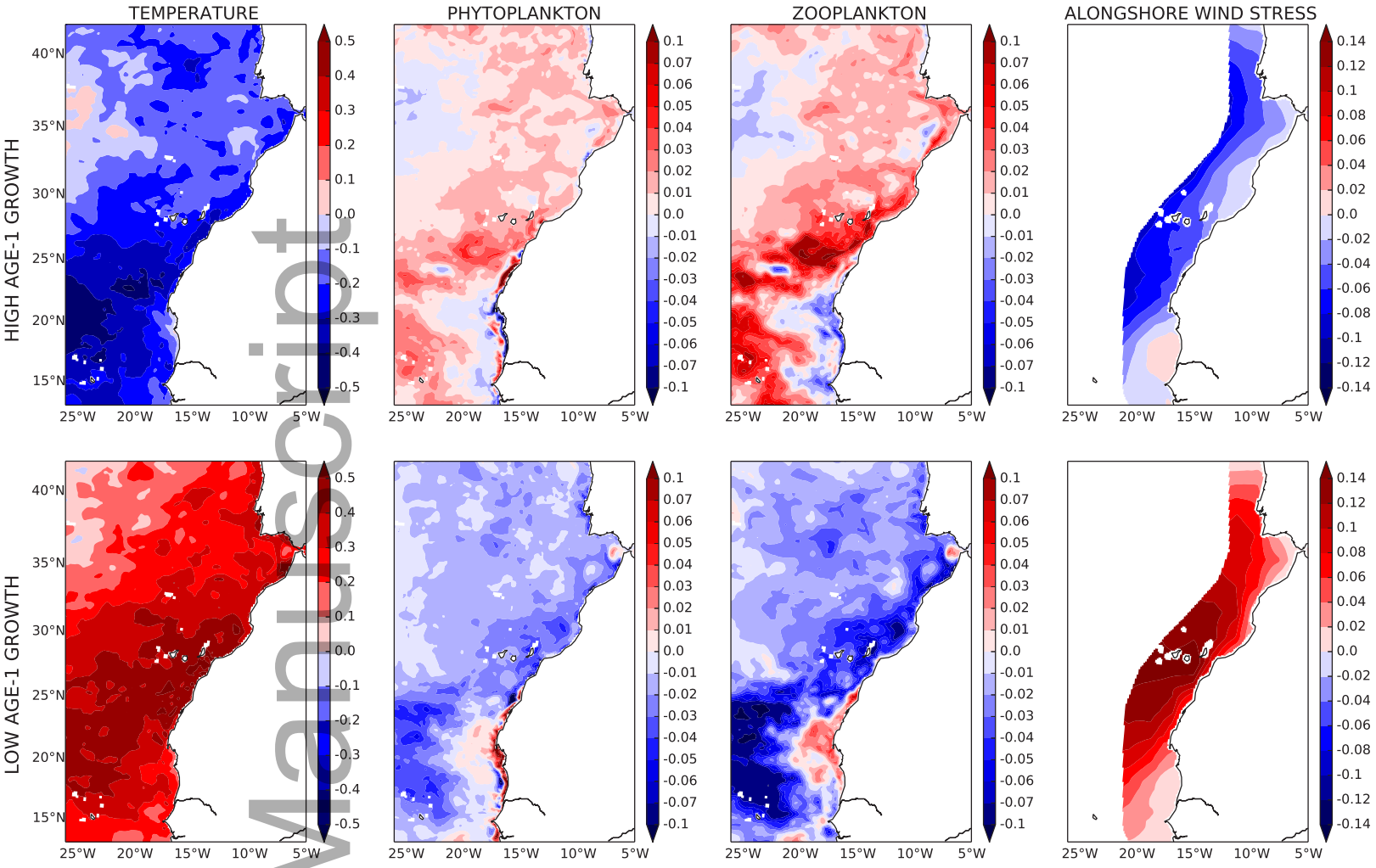

fog_12516_f12.eps

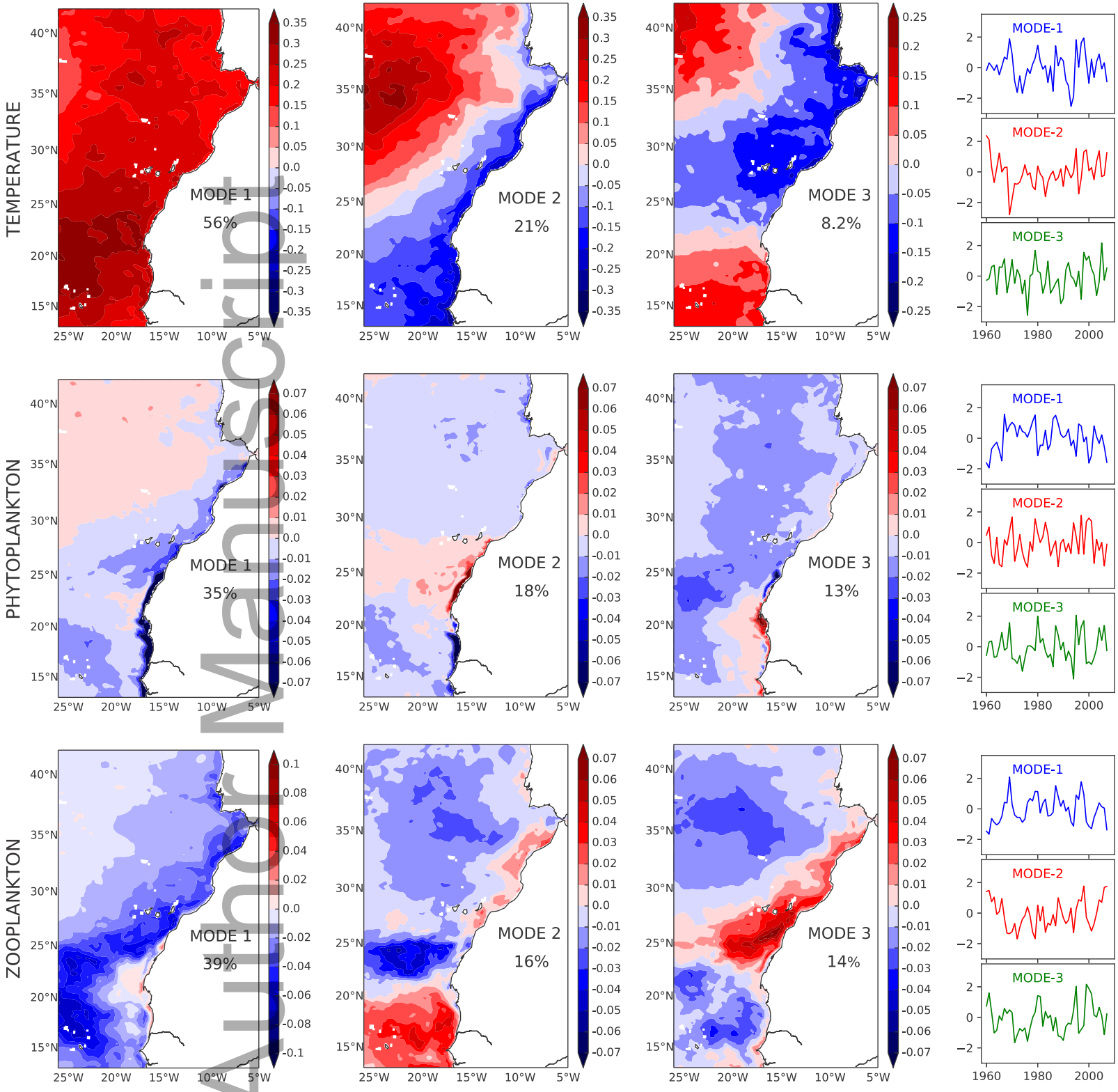

fog_12516_f13.eps

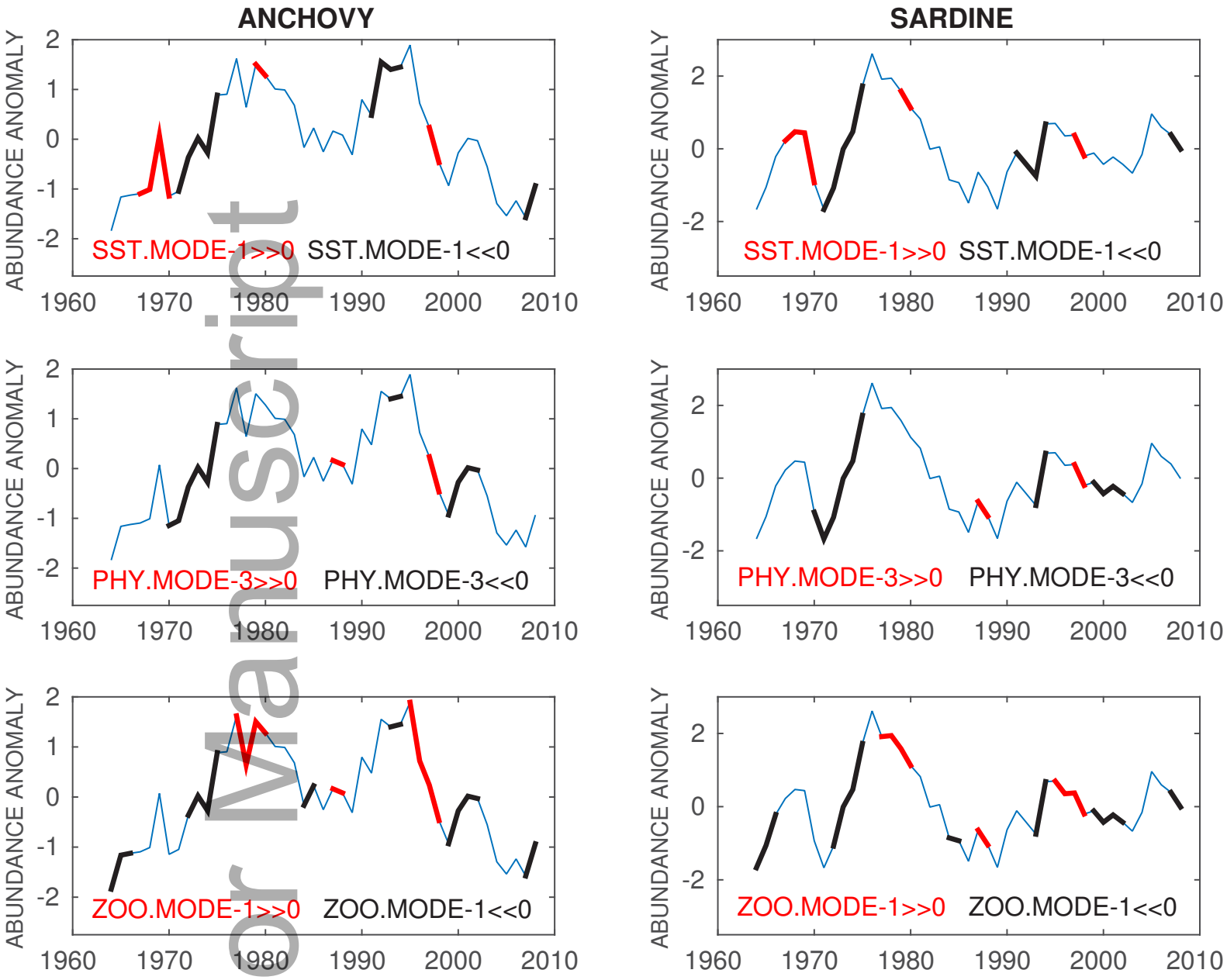

fog_12516_f14.eps

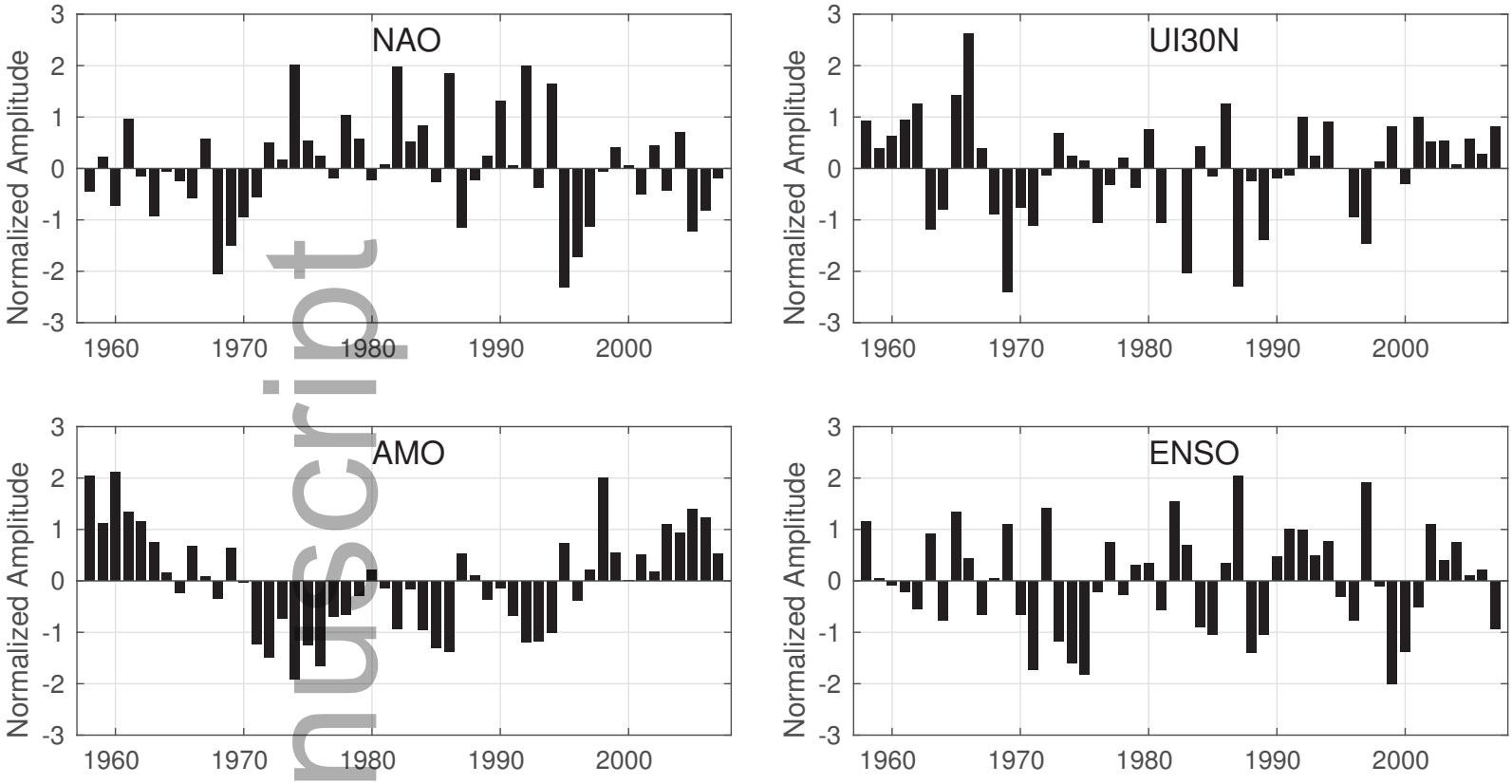

fog_12516_f15.eps

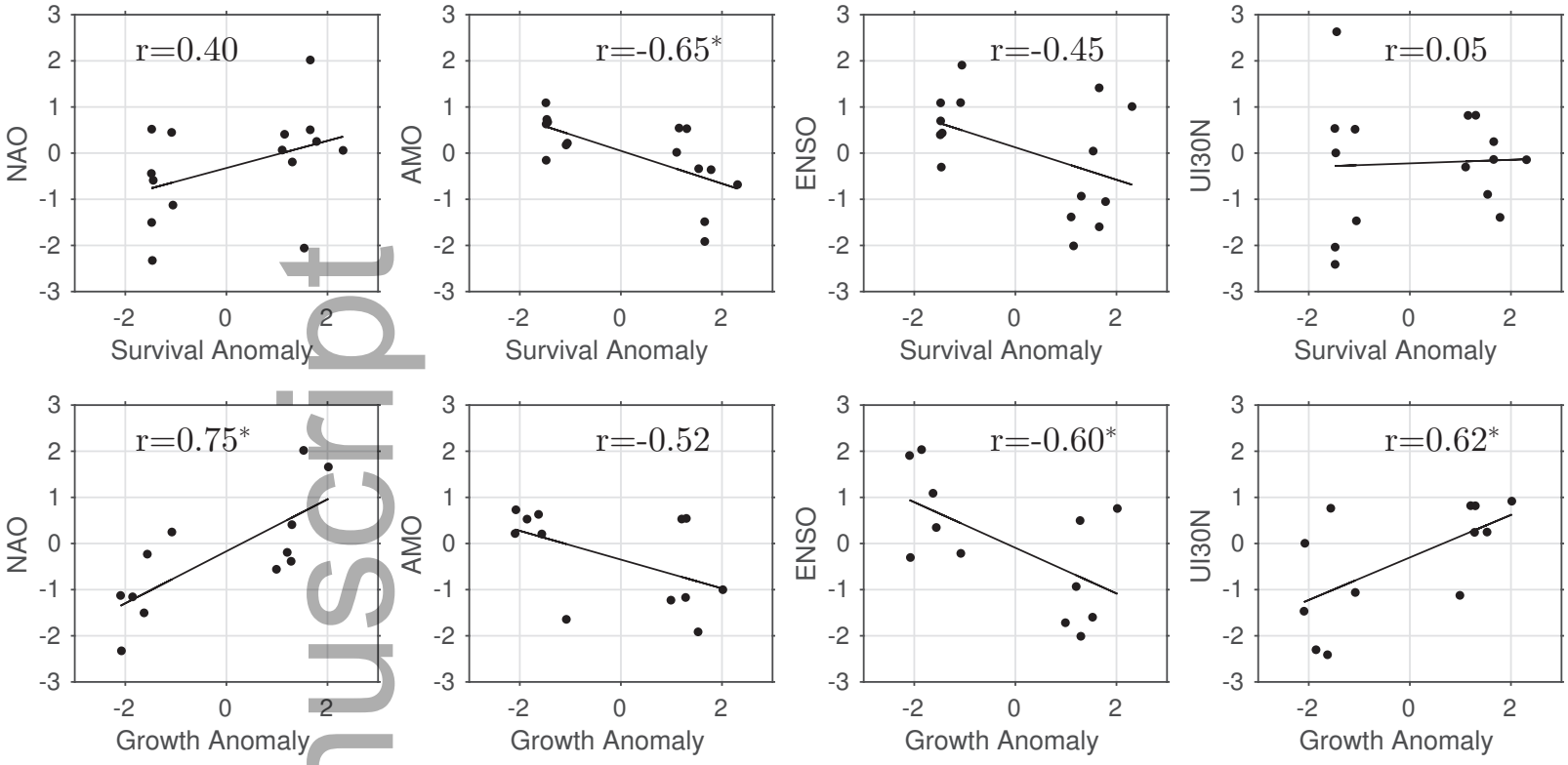

fog_12516_f16.eps

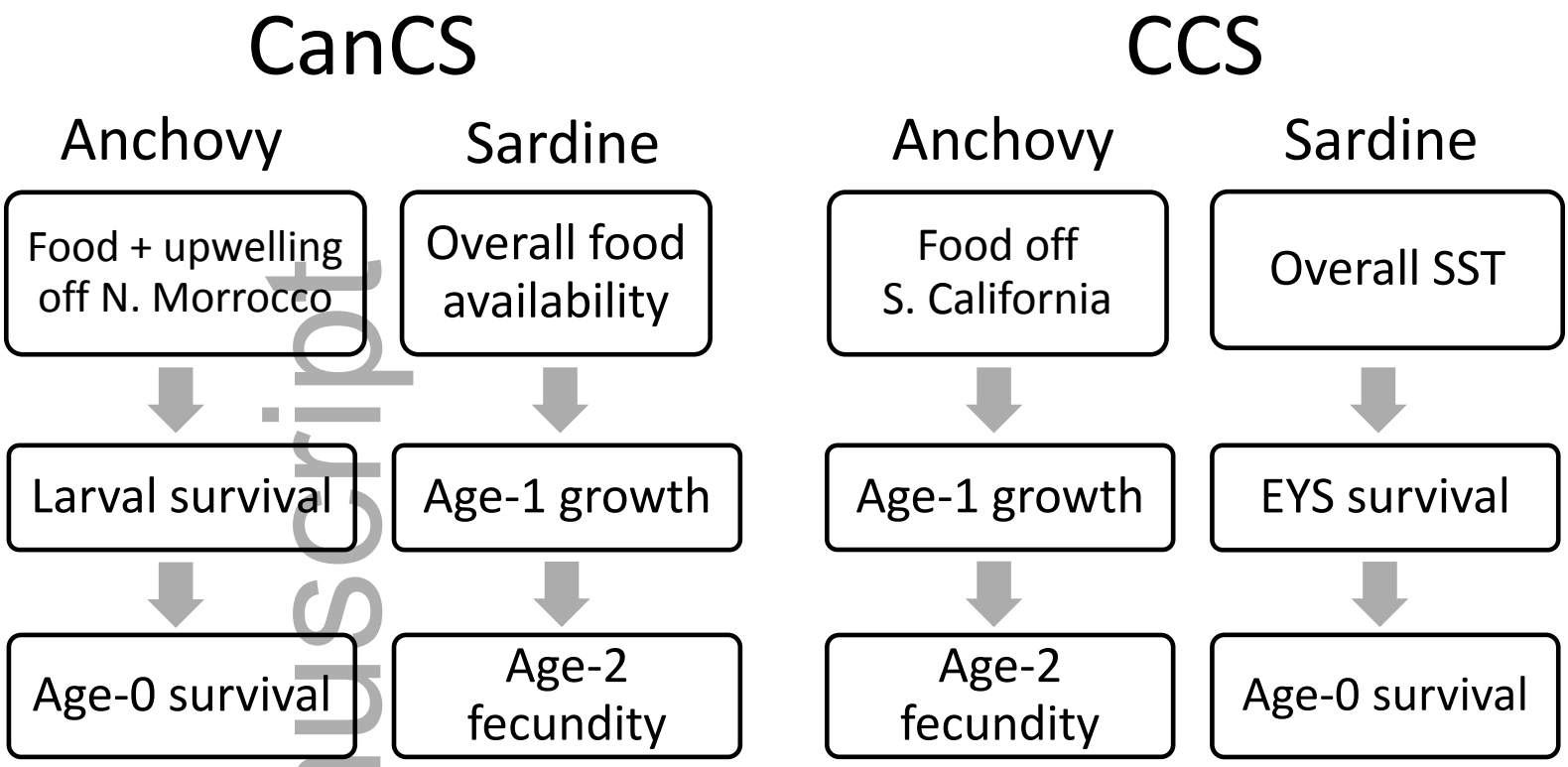

fog_12516_f17.eps

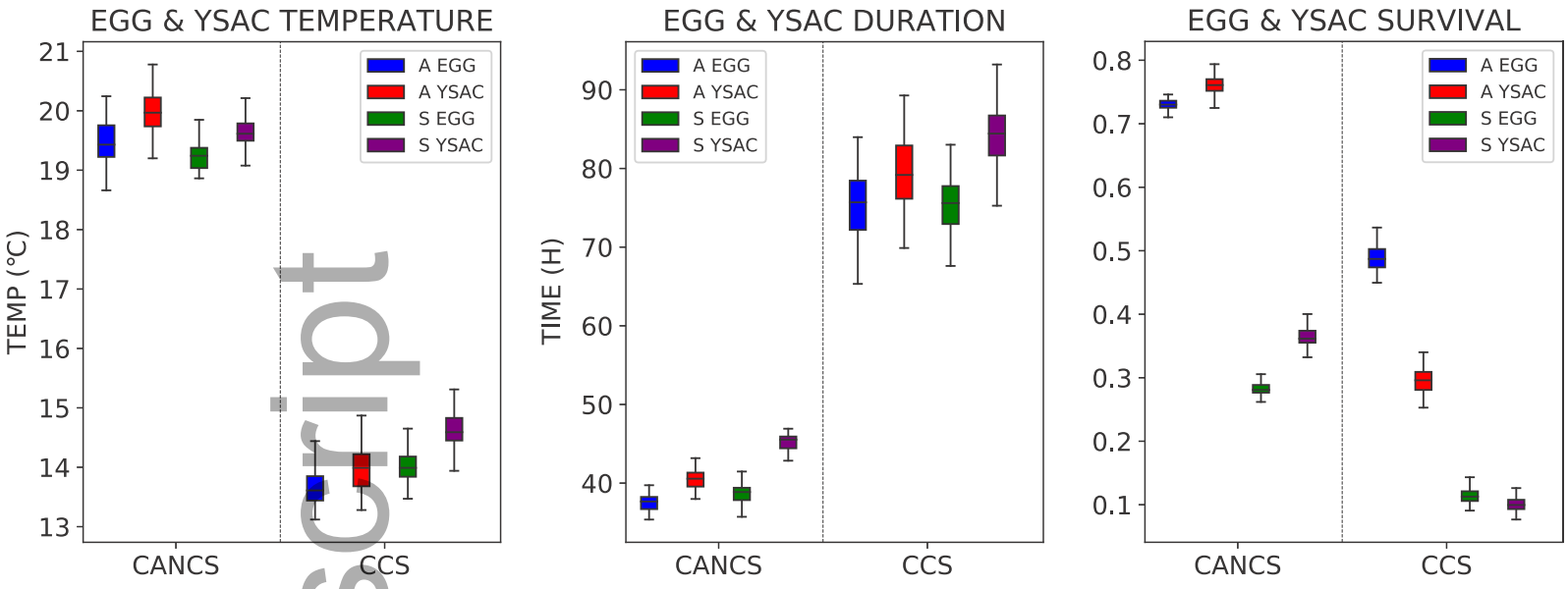

fog_12516_f18.eps